

Bootstrapping from inflationary magnetogenesis to CMB initial conditions

Massimo Giovannini ¹

Department of Physics, Theory Division, CERN, 1211 Geneva 23, Switzerland

INFN, Section of Milan-Bicocca, 20126 Milan, Italy

Abstract

The temperature and polarization anisotropies of the Cosmic Microwave Background are analyzed under the hypothesis that the same inflationary seed accounting for protogalactic magnetism also affects the Einstein-Boltzmann hierarchy whose initial conditions are assigned for typical correlation scales larger than the Hubble radius after matter-radiation equality but before decoupling. Since the primordial gauge spectrum depends on a combination of pivotal parameters of the concordance model, the angular power spectra of the temperature and of the polarization are computed, for the first time, in the presence of a putative large-scale magnetic field of inflationary origin and without supplementary hypotheses.

¹Electronic address: massimo.giovannini@cern.ch

1 Bootstrapping large-scale magnetism

More than sixty years ago, an intense debate on the origin of galactic cosmic rays [1, 2] and the first ambiguous evidences of starlight polarization [3, 4] led Fermi to propose the existence of a galactic magnetic field with approximate strength in the μG range². In the same period it was correctly argued that cosmic rays above 10^{13} eV were galactic (as opposed to solar) and the high degree of isotropy in the arrival directions could be explained by the presence of an irregular magnetic field of μG strength able to scramble the trajectories of charged species (see, for instance, [5] for a terse account of this problem).

Today we know, with a plausible degree of confidence, that the galactic field contains a large-scale regular component and a small-scale turbulent one, both having a local strength of a few μG (see, for instance, [6]). While the turbulent component dominates in strength by a factor of a few, the regular component (with approximate correlation scale between 10 to 30 kpc) imprints dominant drift motions as soon as the Larmor radius of cosmic rays is larger than the maximal scale of the (kinetic or magnetic) turbulences which is $\mathcal{O}(100\text{ pc})$. Clusters (i.e. gravitationally bound systems of galaxies) have been shown to possess a large-scale magnetic field, in the μG range (more specifically between 10 and 100 nG) and with correlation scale larger than in the galactic case suggesting a quasi-flat magnetic power spectrum [7]. Superclusters (i.e. loosely bound systems of clusters) have been also claimed to have magnetic fields [8] at the μG level even if, in this case, unresolved ambiguities persist on the way the magnetic field strengths are inferred from the Faraday rotation measurements.

In a seemingly different perspective we are now facing a problem conceptually close to the one of the early fifties of the past century. The spectrum of the highest energy cosmic rays shows no significant deviation from isotropy [9] as it can be argued from the distribution of arrival directions of cosmic rays detected above 10^{18} eV at the Pierre Auger Observatory. Purported correlations between the arrival directions of cosmic rays with energy above 6×10^{19} eV and the positions of active galactic nuclei within 75 Mpc [10] are then statistically insignificant [9]. At smaller energies it has been convincingly demonstrated [10] that overdensities on windows of 5 deg radius (and for energies $10^{17.9}\text{eV} < E < 10^{18.5}\text{eV}$) are compatible with an isotropic distribution. We can then conclude that in the highest energy domain (i.e. energies larger than about 60 EeV), cosmic rays are not appreciably deflected and basically isotropic. As in the the early fifties the isotropy of the cosmic ray spectrum was a simple (thought indirect) evidence of galactic magnetism, it is tempting to speculate that the isotropy of the highest energy cosmic ray tells a similar story on irregular magnetic fields with correlation scales $\mathcal{O}(\text{few Mpc})$ and within a cocoon of 70 Mpc.

The current pieces of evidence confirm the early suggestions of Fermi arguing that large-scale magnetization should somehow be the remnant of the initial conditions of the gravitational collapse of the protogalaxy occurring over typical length-scales $\mathcal{O}(\text{Mpc})$. Harrison

²We shall employ hereunder the conventional prefixes of International System of units i.e. $\mu\text{G} = 10^{-6}$ Gauss, $\text{nG} = 10^{-9}$ Gauss and so on and so forth.

[12] and, with slightly different accents, Zeldovich [13] were among the first ones to propose that the source of magnetism over the largest length-scales could be searched in the pre-decoupling plasma and, since then, various mechanisms have been tailored for the generation of large-scale magnetic fields (see, for instance, [14]). This class of problems has been dubbed some time ago magnetogenesis [15], i.e. the generation of large-scale magnetic fields during the early stages of the evolution of the plasma. Since the magnetic fields must not jeopardize the spatial isotropy of the background geometry, their Fourier modes must be stochastically distributed and characterized by an appropriate power spectrum:

$$\langle \mathcal{B}_i(\vec{q}, \tau) \mathcal{B}_j(\vec{k}, \tau) \rangle = \frac{2\pi^2}{k^3} P_{\mathcal{B}}(k, \tau) P_{ij}(\hat{k}) \delta^{(3)}(\vec{q} + \vec{k}), \quad (1.1)$$

where, following the standard conventions (see e.g. [19]), $P_{\mathcal{B}}(k, \tau)$ is the physical power spectrum, $P_{ij}(\hat{k}) = (\delta_{ij} - \hat{k}_i \hat{k}_j)$ and $\hat{k}_i = k_i/|\vec{k}|$. As it can be easily verified from the definition of the Fourier transform, $P_{\mathcal{B}}(k, \tau)$ has dimensions of an energy density and its square root has, therefore, the dimensions of a field intensity. Since magnetic fields exist over increasing length-scales with almost the same intensity, the parametrization of Eq. (1.1) implies that $P_{\mathcal{B}}(k, \tau)$ can be considered, in the first approximation, as nearly scale-invariant. Incidentally, on a technical ground, the parametrization of Eq. (1.1) follows the same conventions employed when the power spectra of curvature perturbations are assigned at the standard pivot scale $k_p = 0.002 \text{ Mpc}^{-1}$; denoting with $\mathcal{R}(\vec{k}, \tau) \simeq \mathcal{R}_*(\vec{k})$ the constant mode of curvature perturbations on comoving orthogonal hypersurfaces prior to equality, its two point function in Fourier space is

$$\langle \mathcal{R}(\vec{q}) \mathcal{R}(\vec{k}) \rangle = \frac{2\pi^2}{k^3} P_{\mathcal{R}}(k) \delta^{(3)}(\vec{q} + \vec{k}), \quad P_{\mathcal{R}}(k) = \mathcal{A}_{\mathcal{R}} \left(\frac{k}{k_p} \right)^{n_s-1}, \quad (1.2)$$

where, using the WMAP 9yr data alone [16, 17, 18] in the light of the concordance scenario $\mathcal{A}_{\mathcal{R}} = (2.41 \pm 0.10) \times 10^{-9}$ and $n_s = 0.972 \pm 0.013$. As in the magnetic case, the exact scale-invariant limit is realized when $n_s \rightarrow 1$.

Magnetic fields can be produced during a phase of decelerated expansion inside the particle horizon which always grows much faster than the correlation scale of the field. It is then unlikely to obtain, in this case, correlation scales $\mathcal{O}(\text{Mpc})$ at the onset of protogalactic collapse: this is one of the main drawbacks of what is often called, somehow improperly, causal magnetogenesis [19]. Conversely during inflation the Hubble radius is almost constant $\mathcal{O}(H^{-1})$ and it roughly coincides with the event horizon. The correlation scale of a putative magnetic field amplified during inflation evolves much more rapidly than the Hubble radius itself so that the magnetic power spectrum at the end of inflation has an approximate amplitude $\mathcal{O}(H^4)$. In the context of inflationary models the correlation length-scales of the produced magnetic fields range between $\mathcal{O}(k_p^{-1})$ and $\mathcal{O}(k_L^{-1})$ where k_p (see Eq. (1.2)) is the comoving scale at which the power spectrum of curvature perturbations is assigned in standard analyses and $k_L \simeq \mathcal{O}(\text{Mpc}^{-1})$ corresponds to the wavenumber of the gravitational collapse of the protogalaxy.

To make any statement concerning the early evolution of the plasma, the post-inflationary dynamics must be specified within a reasonable degree of accuracy. Direct Cosmic Microwave Background observations [16, 17, 18] (CMB in what follows), light curves of type-Ia supernovae [20, 21] and large-scale galaxy surveys [22] are compatible with a wide class of scenarios arranged around the Λ CDM paradigm where Λ stands for the dark energy component and CDM for the cold dark matter component. The Λ CDM paradigm consists, nominally, of 6 independent parameters which are extracted from the observational data. However, definite statements demand also more stringent assumptions on the origin of the adiabatic mode or on the thermal history of the plasma at least up to energy scales as large as few TeV. A conventional completion of the Λ CDM paradigm consists of a phase of slow-roll inflation with standard thermal history where the post-inflationary evolution is suddenly dominated by radiation down to the scale of matter-radiation equality. In the latter framework the CMB scale left the inflationary Hubble radius around 65 efolds prior to the end of inflation; conversely the scale of the protogalactic collapse left the inflationary Hubble radius around 9 efolds after the CMB scale.

The conventional completion of the Λ CDM paradigm implies that the typical wavenumber of the gravitational collapse of the protogalaxy in units of the inflationary Hubble rate is:

$$\frac{k_L}{aH} = 3.22 \times 10^{-25} \left(\frac{k_L}{\text{Mpc}^{-1}} \right) \left(\frac{\epsilon}{0.01} \right)^{-1/4} \left(\frac{\mathcal{A}_R}{2.41 \times 10^{-9}} \right)^{-1/4}, \quad (1.3)$$

where, besides \mathcal{A}_R , $\epsilon = -\dot{H}/H^2$ defines the standard slow-roll parameter. The quasi flat spectrum of inflationary origin at the present time and for a typical comoving scale $\mathcal{O}(k_L)$ can then be fully specified in terms of the standard thermal history and it is given by³

$$P_B(k_L, \tau_0) = 10^{-2.43} \left(\frac{\mathcal{A}_R}{2.41 \times 10^{-9}} \right) \left(\frac{\epsilon}{0.01} \right) \left(\frac{h_0^2 \Omega_{R0}}{4.15 \times 10^{-5}} \right) \left(\frac{r}{0.22} \right) \text{ nG}^2, \quad (1.4)$$

where it has been assumed $P_B(k, \tau_{\text{end}}) = rH^4 \simeq \mathcal{O}(H^4)$ at the end of inflation⁴. The magnetic field itself can be estimated by taking the square root of the Eq. (1.4) giving a field of the order of 0.06 nG. Equation (1.4) is compatible with a galactic magnetic field of the order of the μG since during the process of collapse (prior to the onset of galactic rotation) the magnetic flux is frozen into the plasma element thanks to the large value of the conductivity. The mean matter density increases, during collapse, from its critical value (i.e. $\rho_{\text{cr}} = 1.05 \times 10^{-5} h_0^2 \text{GeV}/\text{cm}^3$) to a final value ρ_f value which is 5 to 6 orders of magnitude larger than ρ_c . The magnetic power spectrum after collapse will then be larger than (1.4) by a factor which is roughly $(\rho_f/\rho_c)^{4/3}$.

³Note that $h_0^2 \Omega_R$ corresponds to the present critical fraction of radiation given as the sum of the energy density of the photons and of the neutrinos which are strictly massless in the Λ CDM scenario.

⁴In specific models it turns out that the power spectrum, in the quasi-flat case, is given by rH^4 where r is a numerical factor ranging between 0.1 and 0.01. The reference value of r is $r = 9/(4\pi^2) \simeq 0.22$ and it corresponds to the one obtainable in the context of explicit models mentioned later on.

As a consequence of the standard thermal history, the amplitude of the magnetic power spectrum depends only on ϵ and $\mathcal{A}_{\mathcal{R}}$ and the inflationary Hubble rate in Planck units is given by $H = \sqrt{\pi \epsilon \mathcal{A}_{\mathcal{R}}} M_{\text{P}}$. But since $\mathcal{A}_{\mathcal{R}}$ and $h_0^2 \Omega_{\text{R}}$ are fixed within the vanilla Λ CDM scenario, the amplitude of the seed spectrum effectively depends only on ϵ . The purpose of this paper is to determine the initial conditions of the Einstein-Boltzmann hierarchy in terms of the early initial conditions derivable in the framework of inflationary magnetogenesis. It has been pointed out (see [23] and references therein) that a key role in the analysis of large-scale magnetism must rely on an accurate determination of the distortions induced on the temperature and polarization anisotropies⁵ and various results have been derived both analytically and numerically but never in terms of a primordial inflationary seed. The aim here is to bridge this gap by treating large-scale fields not generically present prior to decoupling but rather coming from inflationary magnetogenesis and to derive the initial conditions of the Einstein-Boltzmann hierarchy. The TT, EE and TE angular power spectra will then be directly computed in terms of the appropriate initial conditions.

To develop a theory of the magnetized initial conditions without running into well known troubles, an efficient tool is the synchronous gauge which is particularly suitable for the perturbative description of the anisotropic stresses. The synchronous results will be explicitly connected to the set of gauge-invariant variables derived by Lukash [24] in the context of the Lifshitz formalism [25] (see also [26, 27]). During the post-inflationary epoch, the evolution of the whole irrotational system is reduced to a single normal mode which is invariant under infinitesimal coordinate transformations (as required in the context of the Bardeen formalism [28]) and whose source terms depend on the magnetic inhomogeneities. In the absence of magnetic fields, earlier analyses [29, 30] followed the same logic of [24] but in the case of scalar field matter. We shall use that the normal modes identified in [24, 29, 30] are all related to the (rescaled) curvature perturbations on comoving orthogonal hypersurfaces [31, 32].

The layout of the present analysis is as follows. In section 2 the fluctuations of inflationary magnetogenesis are analyzed in the synchronous coordinate system. In section 3 the initial conditions of the Einstein-Boltzmann hierarchy are bootstrapped out of the values provided by inflationary magnetogenesis by using the explicit evolution of curvature perturbations for typical scales larger than the Hubble radius at the corresponding epoch. The whole system of perturbations is then integrated across the radiation-matter transition. In section 4 the TT, EE and TE correlations are explicitly computed in the case of a magnetized adiabatic mode of inflationary origin. The B-mode autocorrelations arising in this approach are also briefly examined. Section 5 contains the concluding remarks. In the appendix some of technical results have been collected for the interested reader to avoid excessive digressions.

⁵In the Λ CDM paradigm the temperature and polarization anisotropies are given in terms of the temperature autocorrelations (the TT power spectrum), the polarization autocorrelations (the EE power spectrum) and the temperature-polarization cross-correlations (the TE power spectrum). The other correlations are vanishing even if, in the presence of a stochastic magnetic field, a B-mode power spectrum is naturally induced by Faraday rotation.

2 Inflationary evolution

During a phase of slow-roll dynamics⁶ magnetic fields are amplified while the electric fields are suppressed thanks to the coupling to a spectator field [33, 34, 35]. The electric and magnetic power spectra contribute to the fluctuations of the various components of the energy-momentum tensor and, ultimately, to the curvature perturbations in the same way as a putative magnetic field affects curvature perturbations across the matter radiation transition (see [19] and references therein). The form of the electric and magnetic power spectra will now be discussed not with the aim of endorsing a particular magnetogenesis scenario but with the purpose of drawing general lessons on the parametrization of the magnetized power spectra of curvature perturbations at the end of inflation.

2.1 Parametrization of the power spectra

Consider an explicit coupling of the Abelian kinetic term to a spectator field σ :

$$S = \int d^4x \sqrt{-g} \left[-\frac{1}{2\ell_{\text{p}}^2} R + \frac{1}{2} g^{\alpha\beta} \partial_\alpha \varphi \partial_\beta \varphi - V(\varphi) + \frac{1}{2} g^{\alpha\beta} \partial_\alpha \sigma \partial_\beta \sigma - W(\sigma) - \frac{\lambda(\sigma)}{16\pi} Y_{\mu\nu} Y^{\mu\nu} - j_\mu Y^\mu \right], \quad (2.1)$$

where φ denotes the inflaton field, Y_μ the gauge field, $Y_{\mu\nu}$ the gauge field strength; j_μ represents the potential contribution of an Ohmic current. The evolution of the gauge fields in this class of models has been analyzed in different situations (see, e.g. [33, 34] and references therein). If $\lambda(\sigma)$ is a monotonically increasing function of the conformal time coordinate τ , magnetic fields are amplified while the electric fields are suppressed. This kind of monotonic behavior is quite natural in conventional inflationary models where the curvature scale increases as we approach the protoinflationary stage which is customarily modeled with a phase of decelerated expansion preceding the ordinary slow-roll phase. During the protoinflationary phase conformal invariance can still be unbroken and, if this happens, initial Ohmic currents (remnants of the protoinflationary dynamics) are not dissipated [35]. Conducting initial conditions may then dominate against the quantum initial conditions and the increase of λ corresponds, in this case, to an increase of the Debye shielding length and to a further suppression of the electric fields [35]. For an exponential coupling we shall have, for instance, $\ln \lambda(\sigma) = \gamma_\sigma \sigma / M$ where M is a typical scale characterizing the evolution of the spectator field. The equations of motion of σ can be solved at the level of the background and more specific situations can be found, for instance, in [33] (see also [34]).

⁶Consistently with the absence of spatial curvature of the Λ CDM paradigm, the background geometry is assumed to be conformally flat throughout this investigation; the line element is given by $ds^2 = a^2(\tau)[d\tau^2 - d\vec{x}^2]$. The prime denotes a derivation with respect to the conformal time coordinate τ while the overdot indicates a derivation with respect to the cosmic time coordinate t . The conformal time coordinate τ is related to the cosmic time as $a(\tau)d\tau = dt$.

In a conformally flat background geometry characterized by a scale factor $a(\tau)$ in the conformal time parametrization, the power spectra of the comoving electric and magnetic fields are⁷:

$$P_B(k, \tau) = \frac{k^5}{2\pi^2} |f_k(\tau)|^2, \quad f_k(\tau) = \frac{\mathcal{N}}{\sqrt{2k}} \sqrt{-k\tau} H_\nu^{(1)}(-k\tau), \quad (2.2)$$

$$P_E(k, \tau) = \frac{k^3}{2\pi^2} |g_k(\tau)|^2, \quad g_k(\tau) = -\mathcal{N} \sqrt{\frac{k}{2}} \sqrt{-k\tau} H_{\nu-1}^{(1)}(-k\tau), \quad (2.3)$$

where the mode functions $f_k(\tau)$ and $g_k(\tau)$ are solutions of the corresponding equations⁸:

$$f'_k = g_k + \mathcal{F} f_k, \quad g'_k = -k^2 f_k - \mathcal{F} g_k - 4\pi\sigma_c g_k. \quad (2.4)$$

In Eq. (2.4) the prime denote a derivation with respect to the conformal time coordinate and $\mathcal{F} = \sqrt{\lambda'}/\sqrt{\lambda}$. To keep the discussion general without selecting a specific model, the growth rate \mathcal{F} is parametrized as $\mathcal{F} = f\mathcal{H}$ with $\mathcal{H} = aH$; in the latter case the Bessel index appearing in Eqs. (2.3) and (2.2) is $\nu = 1/2 + f + f\epsilon$ and ϵ is the slow-roll parameter entering the expression of ν since the relation between the Hubble rate and the conformal time coordinate demands the following well known condition $(1 - \epsilon)aH = -\tau$. In the case of Eq. (2.1) $f = \epsilon\gamma_\sigma/(1 - \epsilon)$ but the parametrization in terms of the growth rate has the advantage of being sufficiently general to incorporate at once different dynamical situations. The quasi-flat magnetic spectrum corresponds to the case $f \simeq 2$; direct analyses of these scenarios show that, in this class of models, the departure from scale-invariance cannot be too large (i.e. $f \leq 2.2$) [36] if the adiabatic mode is to be the dominant source of inhomogeneities across matter-radiation decoupling. After the end of inflation $\mathcal{F} \rightarrow 0$ and the relation between the physical and the comoving power spectra is given by $P_B(k, \tau) = a^4(\tau)P_{\mathcal{B}}(k, \tau)$ and $P_E(k, \tau) = a^4(\tau)P_{\mathcal{E}}(k, \tau)$.

As discussed in appendix A the fields $\vec{B}(\vec{x}, \tau)$ and $\vec{E}(\vec{x}, \tau)$ correspond to the canonical normal modes of the system diagonalizing the Hamiltonian density and having well defined properties of transformation under the duality symmetry [35, 37, 38]. In terms of the power spectra of the comoving magnetic and electric fields the correlation functions are given by

$$\langle B_i(\vec{q}, \tau) B_j(\vec{p}, \tau) \rangle = \frac{2\pi^2}{q^3} P_B(q, \tau) P_{ij}(\hat{q}) \delta^{(3)}(\vec{q} + \vec{p}), \quad (2.5)$$

$$\langle E_i(\vec{q}, \tau) E_j(\vec{p}, \tau) \rangle = \frac{2\pi^2}{q^3} P_E(q, \tau) P_{ij}(\hat{q}) \delta^{(3)}(\vec{q} + \vec{p}). \quad (2.6)$$

In full analogy with the power spectra of curvature perturbations introduced in section 1,

⁷Note that $H_\nu(z)$ are standard Hankel functions. Furthermore $|\mathcal{N}|^2 = \pi/2$.

⁸The presence of the conductivity σ_c (not to be confused with the spectator field) plays a specific role during reheating and in the case of conducting initial conditions. More details on these issues can be found in [35]. Here we shall focus, for illustration, on the conventional case of quantum mechanical initial conditions, as it can be argued from the boundary conditions imposed on the mode functions.

the magnetic power spectra can be expressed as

$$P_B(k, \tau) = A_B(k_L, \tau) \left(\frac{k}{k_L} \right)^{n_B-1}, \quad n_B = 5 - 2f - 2f\epsilon,$$

$$A_B(k_L, \tau) = \frac{9 H^4}{4\pi^2} \left(\frac{a_1}{a} \right)^4 \left(\frac{k_L}{aH} \right)^{n_B-1} \mathcal{K}(n_B), \quad \mathcal{K}(n_B) = \frac{2^{5-n_B}}{9\pi} \Gamma^2\left(\frac{6-n_B}{2}\right), \quad (2.7)$$

where (k_L/aH) , as already stressed after Eq. (1.3), in the Λ CDM scenario, is solely determined in terms of ϵ and \mathcal{A}_R . In Eq. (2.7) $\mathcal{K}(n_B)$ varies very little⁹ in the range of physical rates $2 \leq f < 2.2$; for values $f > 2.2$ (excluded from the present considerations) the energy density fluctuations induced by the magnetic fields will get larger than the adiabatic mode. The amplitude $A_B(k_L, \tau)$ depends on the thermal history through the factor (a_1/a) which gets different values depending on the epoch at which the power spectrum is evaluated, for instance, at equality,

$$\left(\frac{a_1}{a_{\text{eq}}} \right) = \left(\frac{2\Omega_{R0}}{\pi\epsilon\mathcal{A}_R} \right)^{1/4} \sqrt{\frac{H_0}{M_P}} \left(\frac{\Omega_{M0}}{\Omega_{R0}} \right) \quad (2.8)$$

where $h_0^2\Omega_{R0} = 4.15 \times 10^{-5}$ and the total matter fraction at the present time is $\Omega_{M0} = \Omega_{c0} + \Omega_{b0}$ is given by the sum of the CDM and of the baryonic contribution. Following the same logic of Eq. (2.8), but at a different redshift, Eq. (1.4) can be derived from Eq. (2.7) by recalling known conversion factors between different system of units¹⁰.

The parameters of Eq. (2.8) can all be extracted, assuming the Λ CDM model, by using different data sets [16, 17, 18] (see also e.g. Eqs. (4.3)–(4.5) in section 4). The only exception is represented by ϵ which cannot be determined in the vanilla Λ CDM model but it can be bounded from above in terms the tensor to scalar ratio $r_T = \mathcal{P}_T/\mathcal{P}_R$ measuring the ratio between the spectrum of the tensor modes and the spectrum of the curvature perturbations at the pivot scale k_p . To first-order in the slow-roll expansion the tensor to scalar ratio $r_T = 16\epsilon + \mathcal{O}(\epsilon^2)$ so that any bound on r_T can be translated into a bound on ϵ . The

Data	r_T	n_s	ϵ
WMAP9 alone	< 0.38	0.992 ± 0.019	< 0.023
WMAP9 + Hubble	< 0.34	0.995 ± 0.015	< 0.021
WMAP9+ BAO	< 0.18	0.973 ± 0.011	< 0.011
WMAP9+ all	< 0.13	$0.9647^{+0.0083}_{-0.0084}$	< 0.0081

Table 1: The upper limits on the tensor-to-scalar ratio and on the slow-roll parameter for some illustrative choices of cosmological data sets.

WMAP9 observations can be combined with different data sets in the light of the Λ CDM scenario supplemented by the tensor modes of the geometry. In this way it is possible to

⁹Note that $\mathcal{K}(1) = 1$.

¹⁰It is useful, for numerical estimates, to appreciate that $M_P^2 = 2.149 \times 10^{66}$ nG.

obtain a bound on r_T and on ϵ . In Tab. 1 the bound on r_T obtainable in the case of the WMAP9 data alone is compared with the same bound obtained by combining the WMAP9 data with the measurements on the Hubble constant of Ref. [43] or by combining the WMAP9 observations with the baryon acoustic oscillations, dubbed BAO in Tab. 1 (see e.g. [22]). The last row of Tab. 1 refers to the combination of the WMAP9 data with almost all the data sets recently available, namely, the data on the Hubble rate, the ones on the baryon acoustic oscillations supplemented by the ones of the Atacama Cosmology Telescope [44], by the data of the south pole telescope [45] and by the three year sample of the supernova legacy survey [46].

For the standard thermal history with sudden reheating also the conductivity σ_c jumps at a finite value at the end of inflation and the continuity of the electric and magnetic fields implies that the amplitude of the electric power spectrum gets suppressed, at a fixed time, as $(k/\sigma_c)^2$ in comparison with its magnetic counterpart [35]. The electric mode functions are exponentially suppressed, for a fixed wavenumber. The magnetic power spectrum is also suppressed, for sufficiently large k , as $\exp[-2(k^2/k_\sigma^2)]$ where $k_\sigma^{-2} = \int_{\tau_\sigma}^\tau d\tau' / [4\pi\sigma_c(\tau')]$. The evaluation of k_σ is complicated by the fact that the integral extends well after τ_σ . This estimate can be made rather accurate by computing the transport coefficients of the plasma in different regimes [47]. By taking $\tau = \tau_{\text{eq}}$

$$\left(\frac{k}{k_\sigma}\right)^2 = \frac{4.75 \times 10^{-26}}{\sqrt{2 h_0^2 \Omega_{\text{M}0} (z_{\text{eq}} + 1)}} \left(\frac{k}{\text{Mpc}^{-1}}\right)^2, \quad (2.9)$$

showing that $\exp[-2(k/k_\sigma)^2]$ is so small to give negligible suppression for $\mathcal{O}(k_p) \leq k \leq \mathcal{O}(k_L)$ where the present considerations apply.

2.2 Energy density and anisotropic stress

The normalized fluctuation of the magnetic energy density and of the related anisotropic stress are given by:

$$\delta\rho_B(\vec{x}, \tau) = \int \frac{d^3q}{(2\pi)^{3/2}} \delta\rho_B(\vec{q}, \tau) e^{-i\vec{q}\cdot\vec{x}}, \quad \Pi_{ij}^{(B)}(\vec{x}, \tau) = \int \frac{d^3q}{(2\pi)^{3/2}} \Pi_{ij}^{(B)}(\vec{q}, \tau) e^{-i\vec{q}\cdot\vec{x}}, \quad (2.10)$$

The normalized fluctuation of the magnetic pressure is $\delta p_B(\vec{x}, \tau) = \delta\rho_B(\vec{x}, \tau)/3$. Since we shall be dealing with the scalar modes of the geometry, it is practical to introduce the scalar projections of the anisotropic stress

$$\nabla^2 \Pi_B(\vec{x}, \tau) = \partial_i \partial_j \Pi_B^{ij}(\vec{x}, \tau). \quad (2.11)$$

The fluctuations of the energy density and of the anisotropic stress in Fourier space are reported in appendix A to avoid lengthy digressions since this analysis is standard and can be found within slightly different perspectives in [19, 23, 36]. In full analogy with the magnetic

fluctuations the fluctuations of the electric energy density and of the electric anisotropic stress can be defined.

The magnetic energy density and the anisotropic stress induce scalar fluctuations of the geometry as established long ago (see [19] and references therein). The variables $h(k, \tau)$ and $\xi(k, \tau)$ parametrize the metric fluctuations in the synchronous coordinate system

$$\delta_s g_{ij}(k, \tau) = a^2 \left[\hat{k}_i \hat{k}_j h + 6\xi \left(\hat{k}_i \hat{k}_j - \frac{\delta_{ij}}{3} \right) \right], \quad \delta_s g_{0i}(k, \tau) = \delta_s g_{00}(k, \tau) = 0, \quad (2.12)$$

where δ_s stresses that we are here considering the scalar modes of the geometry. For practical reasons, in what follows, this subscript will be omitted.

The evolution of $h(k, \tau)$ and $\xi(k, \tau)$ can be obtained by perturbing the Einstein equations during the inflationary phase:

$$-2k^2\xi + \mathcal{H}h' = -4\pi G a^2 (\delta\rho_\varphi + \delta\rho_\sigma + \delta\rho_B), \quad (2.13)$$

$$h'' + 2\mathcal{H}h' - 2k^2\xi = 24\pi G a^2 (\delta p_\varphi + \delta p_\sigma + \delta p_B), \quad (2.14)$$

$$(h + 6\xi)'' + 2\mathcal{H}(h + 6\xi)' - 2k^2\xi = 24\pi G a^2 \Pi_B, \quad (2.15)$$

$$k^2\xi' = -4\pi G [\varphi' k^2 \chi_\varphi + \sigma' k^2 \chi_\sigma - P], \quad (2.16)$$

where χ_φ and χ_σ denote, respectively, the fluctuations of φ and of σ . Equations (2.13) and (2.16) come, respectively, from the (00) and (0i) components of the perturbed Einstein equations. Equations (2.14) and (2.15) are derived from ($i = j$) and ($i \neq j$) components of the perturbed Einstein equations. In Eqs. (2.15) and (2.16) the three-divergence of both sides of the equations has been taken. Finally, in Eq. (2.16) $P(k, \tau)$ denotes the Fourier transform of the three-divergence of the Poynting vector¹¹, i.e. $\vec{\nabla} \cdot [\vec{E} \times \vec{B}]/(4\pi a^4)$. The electric fields have been neglected since they are suppressed all along the inflationary phase.

In the synchronous gauge description, the fluctuations of the energy density and pressure of φ and σ are:

$$\delta\rho_\varphi = \frac{1}{a^2} \left[\varphi' \chi'_\varphi + \frac{\partial V}{\partial \varphi} a^2 \chi_\varphi \right], \quad \delta\rho_\sigma = \frac{1}{a^2} \left[\sigma' \chi'_\sigma + \frac{\partial W}{\partial \sigma} a^2 \chi_\sigma \right], \quad (2.17)$$

$$\delta p_\varphi = \frac{1}{a^2} \left[\varphi' \chi'_\varphi - \frac{\partial V}{\partial \varphi} a^2 \chi_\varphi \right], \quad \delta p_\sigma = \frac{1}{a^2} \left[\sigma' \chi'_\sigma - \frac{\partial W}{\partial \sigma} a^2 \chi_\sigma \right]. \quad (2.18)$$

The fluctuations of the inflaton and of the spectator field obey, respectively, the following two equations:

$$\chi_\varphi'' + 2\mathcal{H}\chi_\varphi' + k^2\chi_\varphi + \frac{\partial^2 V}{\partial \varphi^2} a^2 \chi_\varphi - \frac{\varphi'}{2} h' = 0, \quad (2.19)$$

$$\chi_\sigma'' + 2\mathcal{H}\chi_\sigma' + k^2\chi_\sigma + \frac{\partial^2 W}{\partial \sigma^2} a^2 \chi_\sigma - \frac{\varphi'}{2} h' + \frac{\lambda_{,\sigma}}{\lambda} \delta\rho_B = 0. \quad (2.20)$$

¹¹While P can be neglected in comparison with the other contributions of the momentum constraint, $P' = -4\mathcal{H}P + k^2(\delta\rho_B - 3\Pi_B)/3$. Even if P has been neglected in the final expressions, its derivative has been used whenever needed.

2.3 Curvature perturbations

The system of the perturbed Einstein equations (2.13)–(2.16) supplemented by Eqs. (2.19) and (2.20) can be decoupled in terms of two variables defined as:

$$q_\varphi = a\chi_\varphi - z_\varphi\xi, \quad , \quad q_\sigma = a\chi_\sigma - z_\sigma\xi, \quad (2.21)$$

where $z_\varphi = a\varphi'/\mathcal{H}$ and $z_\sigma = a\sigma'/\mathcal{H}$. The evolution equation obeyed by q_φ and q_σ are obtained from Eqs. (2.19) and (2.20) with the help of Eqs. (2.13) and (2.16). The general result can be further simplified under the assumption that the energy density of σ can be neglected in comparison with the energy density of the inflaton. Defining the rescaled Planck mass¹² the Friedmann equations

$$3\overline{M}_P^2 \mathcal{H}^2 = \frac{1}{2}(\varphi'^2 + \sigma'^2) + a^2 V(\varphi) + a^2 W(\sigma), \quad 2\overline{M}_P^2 (\mathcal{H}^2 - \mathcal{H}') = \varphi'^2 + \sigma'^2, \quad (2.22)$$

imply that the evolution equations for q_φ and q_σ can be expressed as

$$q_\varphi'' + k^2 q_\varphi - \frac{z_\varphi''}{z_\varphi} q_\varphi + \frac{a^3}{\overline{M}_P} \overline{S}_\varphi(k, \tau) = 0, \quad (2.23)$$

$$q_\sigma'' + k^2 q_\sigma - \frac{a''}{a} q_\sigma + \frac{a^3}{\overline{M}_P} \overline{S}_\sigma(k, \tau) = 0. \quad (2.24)$$

Equations (2.23) and (2.24) hold under the approximation that $z_\sigma \ll z_\varphi$ (as implied by the occurrence that $\sigma' \ll \varphi'$); the source terms in Eqs. (2.23) and (2.24) are given by

$$\overline{S}_\varphi(\vec{k}, \tau) = \frac{\varphi'}{3\overline{M}_P \mathcal{H}} \delta\rho_B(\vec{k}, \tau) + \frac{\varphi'}{2\overline{M}_P \mathcal{H}} \Pi_B(\vec{k}, \tau), \quad (2.25)$$

$$\overline{S}_\sigma(\vec{k}, \tau) = \left(\frac{\sigma'}{3\overline{M}_P \mathcal{H}} + \overline{M}_P \frac{\lambda_{,\sigma}}{\lambda} \right) \delta\rho_B(\vec{k}, \tau) + \frac{\sigma'}{2\overline{M}_P \mathcal{H}} \Pi_B(\vec{k}, \tau). \quad (2.26)$$

The curvature perturbations on comoving orthogonal hypersurfaces are expressible, in the synchronous gauge, solely in terms of ξ and of its first time derivative, i.e.

$$\mathcal{R} = \xi + \frac{\mathcal{H} \xi'}{\mathcal{H}^2 - \mathcal{H}'}. \quad (2.27)$$

Using then Eq. (2.16) into Eq. (2.27) to eliminate ξ' and recalling Eq. (2.21), $\mathcal{R}(\vec{k}, \tau)$ becomes:

$$\mathcal{R}(\vec{k}, \tau) \equiv -\frac{z_\varphi(\tau) q_\varphi(\vec{k}, \tau) + z_\sigma(\tau) q_\sigma(\vec{k}, \tau)}{z_\varphi^2(\tau) + z_\sigma^2(\tau)} \simeq -\frac{q_\varphi(\vec{k}, \tau)}{z_\varphi(\tau)} - q_\sigma(\vec{k}, \tau) \frac{z_\sigma(\tau)}{z_\varphi^2(\tau)}, \quad (2.28)$$

where the second equality follows again in the limit $z_\sigma \ll z_\varphi$. Equations (2.25) and (2.26) are easily solvable with standard Green's functions methods when the relevant wavelengths are

¹²In the present paper we shall use both M_P and \overline{M}_P . The two quantities are equal up to the factor $\sqrt{8\pi}$, i.e. $\overline{M}_P = M_P/\sqrt{8\pi} = 1/\sqrt{8\pi G}$.

larger than the Hubble radius during inflation; the result of this procedure can be written as

$$q_\varphi(\vec{k}, \tau) = q_\varphi^{(1)}(\vec{k}, \tau) - \overline{M}_P \left[c_\varphi \Omega_B(\vec{k}, \tau) + d_\varphi \Omega_{B\Pi}(\vec{k}, \tau) \right] a(\tau), \quad (2.29)$$

$$q_\sigma(\vec{k}, \tau) = q_\sigma^{(1)}(\vec{k}, \tau) - \overline{M}_P \left[c_\sigma \Omega_B(\vec{k}, \tau) + d_\sigma \Omega_{B\Pi}(\vec{k}, \tau) \right] a(\tau), \quad (2.30)$$

where the sources have been evaluated to leading order in $k\tau$ and

$$\Omega_B(\vec{k}, \tau) = \frac{\delta\rho_B(\vec{k}, \tau)}{3H^2\overline{M}_P^2}, \quad \Omega_{B\Pi}(\vec{k}, \tau) = \frac{\Pi_B(\vec{k}, \tau)}{3H^2\overline{M}_P^2}. \quad (2.31)$$

In Eqs. (2.29) and (2.30) the following quantities have been introduced

$$c_\varphi = \frac{m(f, \epsilon)}{3\overline{M}_P} \left(\frac{\varphi'}{\mathcal{H}} \right), \quad d_\varphi = \frac{3}{2} c_\varphi \quad (2.32)$$

$$c_\sigma = m(f, \epsilon) \left[\frac{1}{3\overline{M}_P} \left(\frac{\sigma'}{\mathcal{H}} \right) + \overline{M}_P \frac{\lambda_{,\sigma}}{\lambda} \right], \quad d_\sigma = \frac{m(f, \epsilon)}{2\overline{M}_P} \left(\frac{\sigma'}{\mathcal{H}} \right),$$

$$m(f, \epsilon) = \frac{3(1-\epsilon)^2}{(1-2f)(4-2f-3\epsilon)}. \quad (2.33)$$

Using Eq. (2.29) and (2.30) inside Eq. (2.28) the resulting expression for the curvature perturbations can be written as:

$$\mathcal{R}(k, \tau) = \mathcal{R}_*(\vec{k}) + \mathcal{S}_*(\vec{k}) + \mathcal{M}_{\varphi\sigma}^{(B)}(\tau) \Omega_B(k, \tau) + \mathcal{M}_{\varphi\sigma}^{(B\Pi)}(\tau) \Omega_{B\Pi}(k, \tau), \quad (2.34)$$

where $\mathcal{R}_*(\vec{k})$ denotes the standard adiabatic solution associated with $q_\varphi^{(1)}(\vec{k}, \tau)$, $\mathcal{S}_*(\vec{k})$ is the non-adiabatic mode associated with $q_\sigma^{(1)}(\vec{k}, \tau)$:

$$\mathcal{R}_*(\vec{k}) = -\frac{q_\varphi^{(1)}(\vec{k}, \tau)}{z_\varphi(\tau)}, \quad \mathcal{S}_*(\vec{k}) = -q_\sigma^{(1)}(\vec{k}, \tau) \left(\frac{z_\sigma(\tau)}{z_\varphi^2(\tau)} \right). \quad (2.35)$$

The two functions $\mathcal{M}_{\varphi\sigma}^{(B)}(\tau)$ and $\mathcal{M}_{\varphi\sigma}^{(B\Pi)}(\tau)$ are defined as

$$\mathcal{M}_{\varphi\sigma}^{(B)}(\tau) = \frac{\overline{M}_P a(\tau)}{z_\varphi(\tau)} \left[c_\varphi + \left(\frac{z_\sigma}{z_\varphi} \right) c_\sigma \right], \quad \mathcal{M}_{\varphi\sigma}^{(B\Pi)}(\tau) = \frac{\overline{M}_P a(\tau)}{z_\varphi(\tau)} \left[d_\varphi + \left(\frac{z_\sigma}{z_\varphi} \right) d_\sigma \right]. \quad (2.36)$$

The result obtained in Eq. (2.34) has been deduced in rather general terms and it holds, with different forms of the coefficients, not only when the gauge fields are coupled to the spectator field but also when some direct coupling to the inflaton is present. In the forthcoming sections we shall assume the result of Eq. (2.34) and keep the coefficients general. In terms of these coefficients the initial conditions of the Einstein-Boltzmann hierarchy can be derived. In the specific case discussed here the dominant contributions will be the ones of c_φ and d_φ which are, at most, $\mathcal{O}(1/\epsilon)$ in the nearly scale-invariant limit.

2.4 Global variables

There is a conservation law associated with the evolution of \mathcal{R} . Recalling the explicit expression of Eq. (2.27), we can take the first derivative of both sides and use the evolution equations of the fluctuations (2.13)–(2.16) where, instead of specifying the energy densities and the pressures we simply introduce $\delta\rho_t$ (the fluctuation of the total energy density), δp_t (the fluctuation of the total pressure) and the total non-adiabatic pressure fluctuation $\delta p_{\text{nad}} = \delta p_t - c_{\text{st}}^2 \delta\rho_t$ where $c_{\text{st}}^2 = p'_t/\rho'_t$ is the total sound speed of the system; the background pressure and energy density p_t and ρ_t obey the conventional Friedmann equations in the spatially flat case:

$$3\overline{M}_{\text{P}}^2 \mathcal{H}^2 = a^2 \rho_t, \quad 2\overline{M}_{\text{P}}^2 (\mathcal{H}^2 - \mathcal{H}') = a^2 (\rho_t + p_t). \quad (2.37)$$

Equation (2.37) implies $\rho'_t + 3\mathcal{H}(\rho_t + p_t) = 0$. The first derivative of \mathcal{R} turns out to be

$$\mathcal{R}' = -\frac{\mathcal{H}\delta p_{\text{nad}}}{p_t + \rho_t} + \frac{\mathcal{H}\delta\rho_{\text{B}}}{p_t + \rho_t} \left(c_{\text{st}}^2 - \frac{1}{3}\right) + \frac{\mathcal{H}^2(h' + 6\xi')}{8\pi G a^2 (p_t + \rho_t)} - \frac{\mathcal{H} k^2 c_{\text{st}}^2 \xi}{4\pi G a^2 (p_t + \rho_t)} + \frac{\mathcal{H}\Pi_t}{(p_t + \rho_t)}. \quad (2.38)$$

where Π_t denote the total anisotropic stress of the system containing together with the anisotropic stress of the magnetic fields also the anisotropic stress of the other species. In the Λ CDM scenario the other source of anisotropic stress comes from the neutrino sector.

If $\mathcal{S}_*(k) = 0$ in Eq. (2.34), $\delta p_{\text{nad}} = 0$ in Eq. (2.38). This will be the situation considered in the forthcoming section when discussing the magnetized adiabatic mode. Recalling the results of the first paper of Ref. [23], the presence of the non-adiabatic modes can also be easily considered along the lines illustrated above but for the purposes of the present discussion it is unnecessary.

By taking the time derivative of both sides of Eq. (2.38) and from the evolution equations for h and ξ the equation of \mathcal{R} simplifies even further:

$$\mathcal{R}'' + 2\frac{z'_t}{z_t}\mathcal{R}' - c_{\text{st}}^2 \nabla^2 \mathcal{R} = \Sigma'_{\mathcal{R}} + 2\frac{z'_t}{z_t}\Sigma_{\mathcal{R}} + \frac{3a^4}{z^2}\Pi_t, \quad (2.39)$$

where

$$\Sigma_{\mathcal{R}} = -\frac{\mathcal{H}\delta p_{\text{nad}}}{(p_t + \rho_t)} + \frac{\mathcal{H}}{(p_t + \rho_t)} \left[\left(c_{\text{st}}^2 - \frac{1}{3}\right) \delta\rho_{\text{B}} + \Pi_t \right], \quad z_t = \frac{a^2 \sqrt{p_t + \rho_t}}{\mathcal{H} c_{\text{st}}}. \quad (2.40)$$

The results of Eqs. (2.39)–(2.40) reduce, in the absence of magnetic fields and in the absence of anisotropic stress, to the results of Lukash valid in the case of an irrotational relativistic fluid [24, 26, 27]. For wavelengths larger than the Hubble radius the Laplacian of \mathcal{R} can be neglected and the solution of Eq. (2.39) is

$$\mathcal{R}(\vec{x}, \tau) = \mathcal{R}_*(\vec{x}) + \int_{\tau_*}^{\tau} d\tau' \Sigma_{\mathcal{R}}(\vec{x}, \tau') + \int_{\tau_*}^{\tau} \frac{d\tau''}{z_t^2(\tau'')} \int_{\tau_*}^{\tau''} a^4(\tau') \Pi_t(\vec{x}, \tau') d\tau'. \quad (2.41)$$

The continuity of \mathcal{R} across the inflation-radiation transition can be verified in explicit toy models. Consider, for instance, the situation where ρ_t and p_t are both continuous across the inflation-radiation transition. Denoting with $\beta = a/a_*$ the normalized scale factor across the transition, we must require that the effective barotropic index $w_t \rightarrow -1$ and $w_t \rightarrow 1/3$ when β gets, respectively, much smaller and much larger than 1. An interesting interpolating solution of Friedmann equations with this property is given by

$$\rho_t = \frac{12H_*^2 \overline{M}_P^2}{(\beta^2 + 1)^2}, \quad p_t = 4H_*^2 \overline{M}_P^2 \frac{(\beta^2 - 3)}{(\beta^2 + 1)^3}. \quad (2.42)$$

The barotropic index $w_t = (1/3)(\beta^2 - 3)/(\beta^2 + 1)$ goes to $1/3$ for $\beta \gg 1$ and to -1 for $\beta \ll 1$. In conformal time the evolution equations can be explicitly integrated with the result that $\mathcal{H} = (\tau^2 + \tau_*^2)^{-1/2}$ and $\beta(\tau) = \left(\tau + \sqrt{\tau^2 + \tau_*^2}\right)$. These expressions can be used to verify the continuity of $\mathcal{R}(\vec{x}, \tau)$ for instance, in Eq. (2.41).

When inflationary magnetic fields and non-adiabatic pressure fluctuations are both vanishing, the initial conditions of the temperature and polarization anisotropies follow from Eqs. (2.39), (2.40) and (2.41). Even if inflationary magnetic fields are absent the total anisotropic stress Π_t receives contribution from the neutrinos. The compatibility of the neutrino anisotropic stress with the other evolution equations implies, in the case of adiabatic initial conditions, the well known result [40, 41] stipulating that $\Pi_t \simeq \mathcal{O}(k^2 \tau^2)$ when the relevant wavelengths are larger than the Hubble radius at the corresponding epoch. Using Eq. (2.41) and the interpolating solution of Eq. (2.42) it can be shown by direct integration that during the radiation epoch $\mathcal{R}(k, \tau) \simeq \mathcal{R}_*(k) \{1 - (4/9)[R_\nu/(4R_\nu + 15)]k^2 \tau^2\}$ where $R_\nu < 1$ is the (massless) neutrino fraction of the radiation plasma. In summary, for adiabatic initial conditions and in the absence of magnetic fields of inflationary origin $\mathcal{R}(k, \tau) \simeq \mathcal{R}_*(k)$ with corrections which are always small for typical wavelengths larger than the Hubble radius. The generalization of this statement to the case when the inflationary seeds are present will be, among other things, the subject of the following section.

3 Initial conditions of the CMB anisotropies

The value of curvature perturbations computed in the previous section will now be used as initial condition for the subsequent post-inflationary evolution. Focussing on the magnetized adiabatic mode the post-inflationary value of curvature perturbations will be parametrized as:

$$\mathcal{R}(k, \tau) = \mathcal{R}_*(\vec{k}) + c_B R_\gamma \Omega_B(k) + d_B R_\gamma \sigma_B(k), \quad (3.1)$$

where c_B and d_B are of the same order and, as discussed before, at most $\mathcal{O}(1/\epsilon)$. In Eq. (3.1) the energy density and the anisotropic stress of the magnetic fields have been rescaled through the energy density of the photons. After neutrino decoupling (occurring approximately

around the MeV) the anisotropic stress of the neutrinos is generated and $\Pi_t(k, \tau)$ can be parametrized, in the Λ CDM scenario, as

$$\Pi_t(k, \tau) = (p_\nu + \rho_\nu)\sigma_\nu(k, \tau) + (p_\gamma + \rho_\gamma)\sigma_B(k), \quad (3.2)$$

where, following the conventions of section 2, σ_ν is related to the anisotropic stress in real space as $\partial_i \partial_j \Pi_\nu^{ij} = (p_\nu + \rho_\nu) \nabla^2 \sigma_\nu$.

3.1 Pre-decoupling plasma

The perturbed Einstein equations for the post-inflationary system of magnetized perturbations include photons, neutrinos, baryons¹³ and CDM particles. The analog of Eqs. (2.13)–(2.16) will then be:

$$2k^2\xi - \mathcal{H}h' = \frac{a^2}{M_P^2}(\delta\rho_t + \delta\rho_B), \quad (3.3)$$

$$h'' + 2\mathcal{H}h' - 2k^2\xi = \frac{3a^2}{M_P^2}(\delta p_t + \delta p_B), \quad (3.4)$$

$$(h + 6\xi)'' + 2\mathcal{H}(h + 6\xi)' - 2k^2\xi = \frac{3a^2}{M_P^2}[(p_\nu + \rho_\nu)\sigma_\nu + (p_\gamma + \rho_\gamma)\sigma_B], \quad (3.5)$$

$$k^2\xi' = -\frac{a^2}{2M_P^2}(p_t + \rho_t)\theta_t, \quad (3.6)$$

where θ_t , $\delta\rho_t$ and δp_t are¹⁴:

$$(p_t + \rho_t)\theta_t = \sum_a (p_a + \rho_a)\theta_a, \quad \delta\rho_t = \sum_a \delta_s \rho_a, \quad \delta p_t = \sum_a \delta_s p_a = w_a \delta_s \rho_a. \quad (3.7)$$

The sums appearing in Eq. (3.7) extend over the four species of the plasma (i.e. photons, neutrinos, baryons and CDM particles) and w_a is the barotropic index of each species. By using the background equations in their general form, i.e. Eq. (2.37), Eqs. (3.3) and (3.6) can also be written in more explicit terms as:

$$2k^2\xi - \mathcal{H}h' = 3\mathcal{H}^2 \left\{ \Omega_R(R_\gamma\delta_\gamma + R_\nu\delta_\nu) + R_\gamma\Omega_R\Omega_B + \Omega_M \left[\left(\frac{\Omega_{c0}}{\Omega_{M0}} \right) \delta_c + \left(\frac{\Omega_{b0}}{\Omega_{M0}} \right) \delta_b \right] \right\}, \quad (3.8)$$

$$k^2\xi' = -2\mathcal{H}^2 \left[\Omega_R R_\nu \theta_\nu + \Omega_R R_\gamma (1 + R_b) \theta_{\gamma b} + \frac{3}{4} \Omega_M \left(\frac{\Omega_{c0}}{\Omega_{M0}} \right) \rho_c \theta_c \right], \quad (3.9)$$

where δ_γ , δ_ν , δ_b and δ_c denote, with obvious notations, the density contrasts of the four species of the plasma.

¹³The evolution of electrons and ions can be described, effectively, in terms of a single fluid called the baryon fluid whose velocity is the center of mass velocity of the electron-ion system. This happens because the Coulomb coupling is always tight, as argued long ago in the pioneering work of Peebles and Yu [39].

¹⁴In Fourier space θ_t and θ_a denote, respectively, the three-divergences of the total velocity field and of the different species composing the plasma.

At sufficiently early times, the velocity of the photons coincides with the baryon velocity, i.e. $\theta_\gamma \simeq \theta_b = \theta_{\gamma b}$ since the photons and the baryons are tightly coupled by Thomson scattering. In the momentum constraint of Eq. (3.9) the tight-coupling regime has been already assumed. Furthermore, because we are going to solve the system across the radiation-matter transition, the Poynting vector can be safely neglected. Using the same strategy leading to Eqs. (3.8) and (3.9), Eqs. (3.4) and (3.5) can be recast in the following form:

$$h'' + 2\mathcal{H}h' - 2k^2\xi = 3\mathcal{H}^2\Omega_R(R_\gamma\delta_\gamma + R_\nu\delta_\nu + R_\gamma\Omega_B) \quad (3.10)$$

$$(h + 6\xi)'' + 2\mathcal{H}(h + 6\xi)' - 2k^2\xi = 12\mathcal{H}^2\Omega_R[R_\nu\sigma_\nu + R_\gamma\sigma_B], \quad (3.11)$$

where, the critical fraction of radiation and of matter are defined as:

$$\Omega_R = \frac{a_e}{a_{\text{eq}} + a}, \quad \Omega_M = \frac{a}{a + a_{\text{eq}}}. \quad (3.12)$$

The initial conditions of the Einstein-Boltzmann hierarchy are fully specified by solving also the equations of the monopoles and the dipoles of the phase-space distribution of the various species. The monopoles are related to the density contrasts whose evolution is given by:

$$\delta'_\nu = -\frac{4}{3}\theta_\nu + \frac{2}{3}h', \quad \delta'_\gamma = -\frac{4}{3}\theta_{\gamma b} + \frac{2}{3}h', \quad (3.13)$$

$$\delta'_b = -\theta_{\gamma b} + \frac{h'}{2}, \quad \delta'_c = -\theta_c + \frac{h'}{2}. \quad (3.14)$$

The equations for the dipoles are related to the peculiar velocity of the various species:

$$\theta'_\nu = \frac{k^2}{4}\delta_\nu - k^2\sigma_\nu, \quad (3.15)$$

$$\theta'_{\gamma b} + \frac{\mathcal{H}R_b}{R_b + 1}\theta_{\gamma b} = \frac{k^2}{4(1 + R_b)}\delta_\gamma + \frac{k^2}{4(1 + R_b)}(\Omega_B - 4\sigma_B), \quad (3.16)$$

$$\theta'_c + \mathcal{H}\theta_c = 0. \quad (3.17)$$

In Eq. (3.15) there appears also σ_ν whose evolution equation is coupled to all the higher multipoles of the neutrino phase-space distribution

$$\sigma'_\nu = \frac{4}{15}\theta_\nu - \frac{3}{10}k\mathcal{F}_{\nu 3} - \frac{2}{15}h' - \frac{4}{5}\xi', \quad (3.18)$$

$$\mathcal{F}'_{\nu\ell} = \frac{k}{2\ell + 1}\left[\ell\mathcal{F}_{\nu(\ell-1)} - (\ell + 1)\mathcal{F}_{\nu(\ell+1)}\right], \quad \ell \geq 3. \quad (3.19)$$

where $\mathcal{F}_{\nu\ell}$ denotes the ℓ th multipole of the perturbed phase-space distribution of the neutrinos. The evolution equations reported here hold prior to photon decoupling. Across decoupling the baryons and the photons obey effectively different equations since the approximation based on the tight photon-baryon coupling breaks down.

3.2 Explicit solutions and magnetized adiabatic mode

The solution of Eq. (2.37) across the radiation-matter transition and for a spatially flat Universe reads:

$$\alpha = \frac{a}{a_{\text{eq}}} = x^2 + 2x, \quad x = \frac{\tau}{\tau_1}, \quad \tau_1 = \frac{2}{H_0} \sqrt{\frac{a_{\text{eq}}}{\Omega_{\text{M}0}}} \simeq 283.73 \left(\frac{h_0^2 \Omega_{\text{M}0}}{0.1368} \right)^{-1} \text{Mpc}, \quad (3.20)$$

where a_{eq} is the scale factor at the equality already introduced in Eq. (3.12), i.e. the moment when non-relativistic matter and radiation contribute equally to the total energy density of the plasma. For $\alpha = \rho_{\text{M}}/\rho_{\text{R}} \ll 1$ (i.e. $a \ll a_{\text{eq}}$) the plasma is dominated by radiation and according to Eq. (3.20), $\alpha \simeq 2x + \mathcal{O}(x^2) = 2(\tau/\tau_1)$.

Defining as τ_1 the initial integration time, it will be required that $k\tau_1 < 1$ for all the modes involved in the calculations. The double expansion employed in setting initial conditions of the truncated Einstein-Boltzmann hierarchy can be formally expressed as¹⁵

$$\alpha \ll 1, \quad \frac{k}{aH} = \frac{k}{\mathcal{H}} = \frac{\kappa \alpha}{2\sqrt{\alpha+1}} \simeq k\tau \ll 1. \quad (3.21)$$

where $\kappa = k\tau_1$ measures how large the wavelength was, in Hubble units, around equality (note, indeed, that $\tau_{\text{eq}} = (\sqrt{2} - 1)\tau_1 \simeq \tau_1/2$).

The initial conditions studied here incorporate the inflationary seeds in the adiabatic mode and belong to the class of the magnetized adiabatic modes (see [19, 23] and references therein). To investigate the time evolution of the system it is useful to employ directly the normalized scale factor α . The initial conditions pertaining to the magnetized adiabatic mode can then be written as:

$$\delta_\nu(\kappa, \alpha_i) \simeq \delta_\gamma(\kappa, \alpha_i) \simeq \frac{3}{4}\delta_{\text{b}}(\kappa, \alpha_i) \simeq \frac{3}{4}\delta_{\text{c}} = -R_\gamma \Omega_{\text{B}}(\kappa, \alpha_i), \quad (3.22)$$

$$\theta_\nu(\kappa, \alpha_i) \simeq \theta_{\gamma\text{b}}(\kappa, \alpha_i) \simeq \theta_{\text{c}}(\kappa, \alpha_i) \simeq 0, \quad (3.23)$$

$$\sigma_\nu(\kappa, \alpha_i) = 0, \quad \mathcal{F}_\ell(\kappa, \alpha_i) = 0, \quad (3.24)$$

where α_i denotes the initial integration variable and $\ell \geq 3$. In the synchronous gauge, the density contrasts on uniform curvature hypersurfaces are defined as $\zeta_{\text{a}} = \xi + \delta_{\text{a}}/[3(w_{\text{a}} + 1)]$. But then, the conditions (3.22) imply that all the ζ_{a} must be equal, i.e. $\zeta_\nu = \zeta_\gamma = \zeta_{\text{c}} = \zeta_{\text{b}}$ for $\alpha = \alpha_i$ and $\kappa < 1$. In this sense the initial conditions (3.22)–(3.24) generalize the adiabatic mode to the situation where inflationary seeds are present¹⁶.

According to Eq. (2.39) the initial conditions (3.22)–(3.24) seem to be compatible with the adiabatic mode only if $\Pi_{\text{t}} \rightarrow 0$. The neutrino anisotropic stress must be zero initially and also its first derivative is zero since $\mathcal{F}_{\nu\ell} = 0$ for $\ell \geq 3$. But thanks to the presence

¹⁵In terms of the solution of Eq. (3.20), $\mathcal{H} = 2\sqrt{\alpha+1}/(\tau_1\alpha)$ and $c_{\text{st}}^2 = 4/(3\alpha+4)$.

¹⁶It should be borne in mind that, in the synchronous gauge, the condition $\theta_{\text{c}} = 0$ is enforced not so much because of a property of the initial data but rather to fix completely the coordinate system and to avoid the occurrence of known spurious (gauge) modes arising in the synchronous description [42]

of the magnetic anisotropic stress, the total anisotropic stress does not vanish even before neutrino decoupling: $\Pi_t(\kappa, \alpha_i) \neq 0$ even if $\sigma_\nu(\kappa, \alpha_i)$ and its derivatives are all vanishing. Direct numerical integration shows that, after a transient time, $\Pi_t \rightarrow 0$ even if, initially, $\Pi_t \neq 0$. This result is established by integrating Eqs. (3.4)–(3.11), (3.13)–(3.14) and (3.15)–(3.19) in the background defined by Eq. (3.20) and subjected to the initial conditions (3.1) and (3.22)–(3.24). In Fig. 1 the evolution of the neutrino anisotropic $\sigma_\nu(\kappa, \alpha)$ stress and

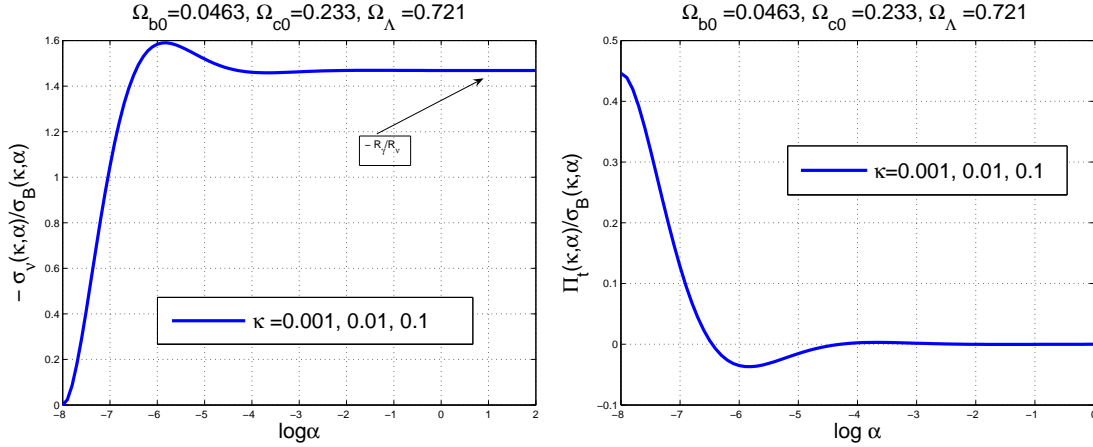


Figure 1: Evolution of the anisotropic stress in the case of the magnetized adiabatic mode. In the left plot the neutrino anisotropic stress is illustrated. In the plot at the right the total anisotropic stress is reported. On the horizontal axes the results are given in terms of the common logarithm of the normalized scale factor.

of the total anisotropic stress $\Pi_t(\kappa, \alpha)$ is illustrated as a function of the common logarithm of the normalized scale factor. On the vertical axis of both plots of Fig. 1 the anisotropic stresses are given in units of the magnetic anisotropic stress $\sigma_B(\kappa)$.

Denoting with R_ν and $R_\gamma = 1 - R_\nu$ the fractions of neutrinos and photons in the pre-decoupling plasma¹⁷, the arrow in the left plot underlines the value $-R_\gamma/R_\nu$ (which is asymptote of σ_ν/σ_B for $k\tau \ll 1$). The result of Fig. 1 can be obtained by integrating directly the system in the α parametrization. The equations are reported, for completeness, in appendix B. As the legends indicate in Fig. 1, different values of κ produce results which are indistinguishable provided $\kappa \ll 1$.

In the limit $\alpha < 1$ and $k\tau < 1$ we can solve consistently the system discussed in the previous section and expressed, in the α -parametrization, in appendix B. The result is:

$$\xi(k, \tau) = \mathcal{R}_*(k) \left[1 - \frac{(4R_\nu + 5)k^2\tau^2}{12(4R_\nu + 15)} \right] + R_\gamma \Omega_B(k) \left[c_B - \frac{R_\nu k^2\tau^2}{6(4R_\nu + 15)} \right]$$

¹⁷In the Λ CDM paradigm $R_\nu = [3 \times (7/8) \times (4/11)^{4/3}] / [1 + 3 \times (7/8) \times (4/11)^{4/3}] = 0.4052$ where 3 counts the massless neutrino families, $(7/8)$ stems from the Fermi-Dirac statistics and $(4/11)^{4/3}$ is related to the different kinetic temperature of neutrinos.

$$+ R_\gamma \sigma_B \left[d_B + \frac{2k^2 \tau^2}{3(4R_\nu + 15)} \right] \quad (3.25)$$

$$\begin{aligned} h(k, \tau) &= \frac{\mathcal{R}_*(k)}{2} k^2 \tau^2 \left[1 + \frac{8R_\nu^2 - 14R_\nu - 75}{36(2R_\nu + 25)(4R_\nu + 15)} k^2 \tau^2 \right] \\ &+ \frac{R_\gamma \Omega_B(k)}{2} k^2 \tau^2 \left[c_B + \frac{R_\nu(20R_\nu - 15)}{180(4R_\nu + 15)(2R_\nu + 25)} k^2 \tau^2 \right] \\ &+ \frac{R_\gamma \sigma_B(k)}{2} k^2 \tau^2 \left[d_B - \frac{R_\nu(20R_\nu - 15)}{45(4R_\nu + 15)(2R_\nu + 25)} k^2 \tau^2 \right]. \end{aligned} \quad (3.26)$$

For the density contrasts we have instead

$$\begin{aligned} \delta_\gamma(k, \tau) &= \frac{\mathcal{R}_*(k)}{3} k^2 \tau^2 - R_\gamma \Omega_B(k) \left[1 - \frac{1}{3} \left(c_B - \frac{R_\nu}{2R_\gamma} \right) k^2 \tau^2 \right] \\ &+ \frac{2}{3} \sigma_B(k) \left[1 + \frac{d_B R_\gamma}{2} \right] k^2 \tau^2 \end{aligned} \quad (3.27)$$

$$\begin{aligned} \delta_\nu(k, \tau) &= \frac{\mathcal{R}_*(k)}{3} k^2 \tau^2 - R_\gamma \Omega_B(k) \left[1 + \left(R_\gamma - 2c_B \right) \frac{k^2 \tau^2}{6} \right] \\ &+ \frac{R_\gamma}{3} \sigma_B(k) \left[d_B - \frac{3}{2R_\nu} \right] k^2 \tau^2 \end{aligned} \quad (3.28)$$

$$\delta_c(k, \tau) = \frac{\mathcal{R}_*(k)}{4} k^2 \tau^2 - \frac{3}{4} R_\gamma \Omega_B(k) \left[1 - c_B \frac{k^2 \tau^2}{3} \right] + \frac{d_B R_\gamma}{4} \sigma_B(k) k^2 \tau^2 \quad (3.29)$$

$$\begin{aligned} \delta_c(k, \tau) &= \frac{\mathcal{R}_*(k)}{4} k^2 \tau^2 - \frac{3}{4} R_\gamma \Omega_B(k) \left[1 - \frac{1}{4} \left(c_B - \frac{R_\nu}{2R_\gamma} \right) k^2 \tau^2 \right] \\ &+ \frac{\sigma_B(k)}{4} k^2 \tau^2 (2 + d_B R_\gamma) \end{aligned} \quad (3.30)$$

For the velocities we have

$$\begin{aligned} \theta_{\gamma b}(k, \tau) &= \frac{k^4 \tau^3}{36} \mathcal{R}_*(k) + \frac{R_\gamma \Omega_B(k)}{4} k^2 \tau \left[1 + \frac{1}{9} \left(c_B \frac{R_\gamma}{R_\nu} - \frac{1}{2} \right) k^2 \tau^2 \right] \\ &- \sigma_B(k) \left[1 + \frac{1}{18} \left(1 - \frac{d_B R_\gamma}{2} \right) k^2 \tau^2 \right] \end{aligned} \quad (3.31)$$

$$\begin{aligned} \theta_\nu(k, \tau) &= \mathcal{R}_*(k) \left(\frac{4R_\nu + 23}{4R_\nu + 15} \right) \frac{k^4 \tau^3}{36} - \frac{R_\gamma \Omega_B(k)}{4} \left[1 - \frac{1}{9} \left(\frac{4R_\nu + 23}{4R_\nu + 15} c_B - \frac{4R_\nu + 27}{2(4R_\nu + 15)} \right) k^2 \tau^2 \right] \\ &+ \sigma_B(k) \frac{R_\gamma}{R_\nu} k^2 \tau \left\{ 1 + \frac{k^2 \tau^2}{18} \left[\frac{4R_\nu + 27}{2(4R_\nu + 15)} + \frac{d_B R_\nu}{2} \left(\frac{4R_\nu + 23}{4R_\nu + 15} \right) \right] \right\} \end{aligned} \quad (3.32)$$

while $\theta_c = 0$. Finally the anisotropic stress of the neutrinos is given by

$$\begin{aligned} \sigma_\nu(k, \tau) &= -\frac{R_\gamma}{R_\nu} \sigma_B(k) - \frac{2\mathcal{R}_*(k)}{3(4R_\nu + 15)} k^2 \tau^2 \\ &- \left[\frac{2}{3(4R_\nu + 15)} \left(c_B + \frac{3}{4} \right) R_\gamma \Omega_B(k) - \frac{2\sigma_B(k)}{(4R_\nu + 15)} \frac{R_\gamma}{R_\nu} \left(1 - \frac{d_B}{3} R_\nu \right) \right] k^2 \tau^2 \end{aligned} \quad (3.33)$$

All the higher multipoles in the neutrino hierarchy have been consistently set to zero since we are concerned here with the adiabatic initial data. Different initial conditions may demand

different assumptions on the higher multipoles of the hierarchy. This analysis closely follows earlier results (see [19, 23] and references therein) where, for the first time, the problem of the magnetized initial conditions of the Einstein-Boltzmann hierarchy has been posed and discussed. The crucial difference is represented by the inflationary origin of the magnetic fields which induces a further contribution on the curvature perturbations and, therefore, on the whole hierarchy. Note that when the magnetized contribution is switched off, the initial conditions of Eqs. (3.25)–(3.33) reproduce the standard adiabatic initial condition discussed long ago (see, e.g. [40]).

4 Temperature and polarization power spectra

The temperature and polarization observables can be obtained by integrating numerically the magnetized Einstein-Boltzmann hierarchy across recombination with the full set of initial conditions discussed from Eq. (3.25) to Eq. (3.33). The Boltzmann integrator employed here is based on the code described in Ref. [19, 23] and used to investigate the magnetized CMB anisotropies. The Boltzmann code is based on Cosmics [40] and on CMBFAST [41] and it includes the evolution of magnetic fields within a consistent magnetohydrodynamical approximation.

The temperature autocorrelations (TT correlations in what follows), the polarization autocorrelations (EE correlations in what follows) and the cross-correlation between the temperature and the polarization (TE correlations in what follows) are defined in the standard standard way (see, for instance, Eqs. (2.61)–(2.63) of the second paper quoted in Ref. [23]). All the different correlation spectra will be expressed in units of $(\mu\text{K})^2$. The following shorthand notation shall be used:

$$\mathcal{G}_\ell^{(\text{TT})} = \frac{\ell(\ell+1)}{2\pi} C_\ell^{\text{TT}}, \quad \mathcal{G}_\ell^{(\text{EE})} = \frac{\ell(\ell+1)}{2\pi} C_\ell^{\text{EE}}, \quad \mathcal{G}_\ell^{(\text{TE})} = \frac{\ell(\ell+1)}{2\pi} C_\ell^{\text{TE}}. \quad (4.1)$$

In the minimal ΛCDM scenario the angular power spectra of Eq. (4.1) are the only non-vanishing observables since the tensor modes are neglected and the B-mode polarization is absent. As we shall argue later, however, a B-mode autocorrelation can be induced, via Faraday effect, from the EE correlations.

The spectra of Eq. (4.1) depend on 6 independent parameters

$$\mathcal{G}_\ell^{(\text{XY})} = \mathcal{G}_\ell^{(\text{XY})}(n_s, \Omega_{\text{b}0}, \Omega_{\text{c}0}, \Omega_\Lambda, H_0, \epsilon_{\text{re}}), \quad (4.2)$$

where ϵ_{re} (not to be confused with the slow-roll parameter) denotes the optical depth at reionization. The pivotal parameters of the ΛCDM paradigm can be determined on the basis of different data sets and, for illustrative purposes, we shall bound the attention only to three best fits. The first one is obtained by comparing the ΛCDM paradigm to the WMAP 9yr data alone (see, in particular, [16]):

$$(\Omega_{\text{b}0}, \Omega_{\text{c}0}, \Omega_{\text{de}0}, h_0, n_s, \epsilon_{\text{re}}) \equiv (0.0463, 0.233, 0.721, 0.700, 0.972, 0.089), \quad (4.3)$$

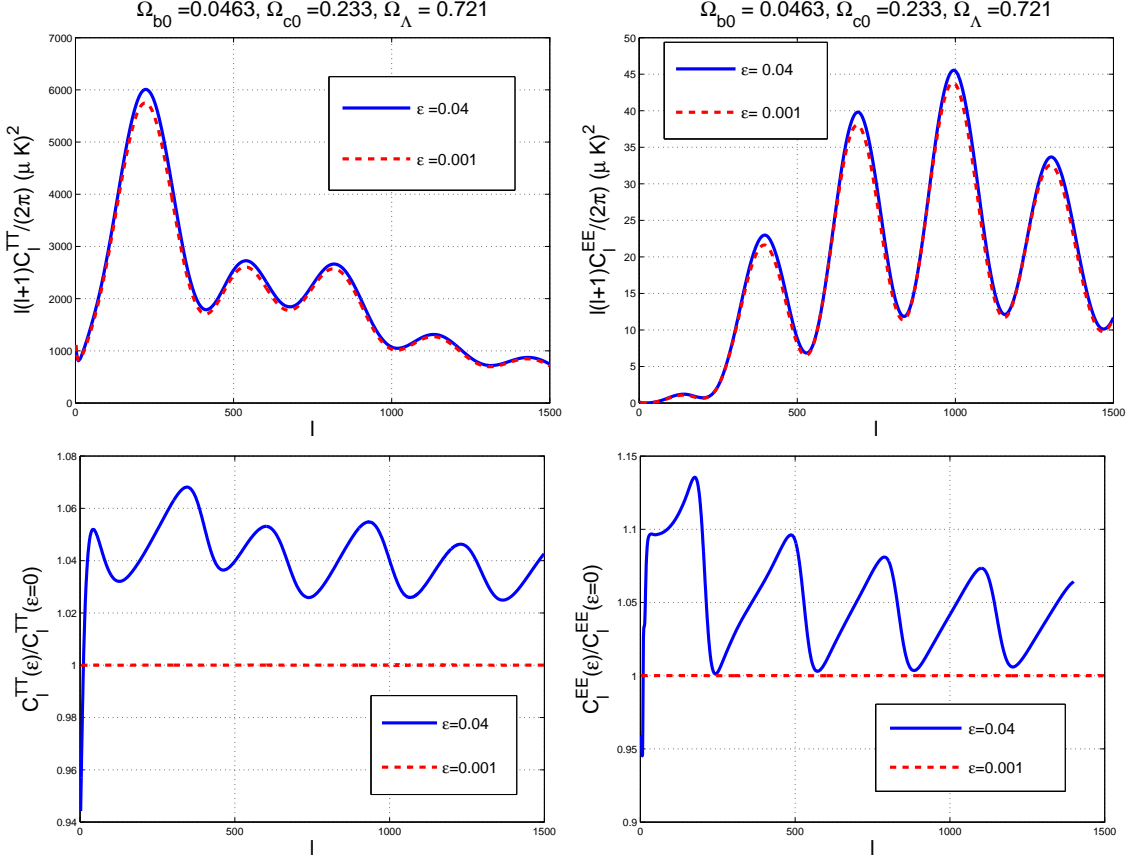


Figure 2: In the two upper plots the TT and the EE correlations are illustrated for the initial conditions of Eqs. (3.1)–(3.33)

with $\mathcal{A}_{\mathcal{R}} = 2.41 \times 10^{-9}$ (recall, in fact, the parametrization introduced in Eq. (1.2)). If we include the data sets pertaining to the baryon acoustic oscillations (see, e.g. [22]) the parameters are slightly different:

$$(\Omega_{b0}, \Omega_{c0}, \Omega_{de0}, h_0, n_s, \epsilon_{re}) \equiv (0.0477, 0.247, 0.705, 0.686, 0.967, 0.086), \quad (4.4)$$

with $\mathcal{A}_{\mathcal{R}} = 2.35 \times 10^{-9}$. Another possible set of parameters considered hereunder is the one obtained by combining the WMAP9 data with the direct determinations of the Hubble rate

$$(\Omega_{b0}, \Omega_{c0}, \Omega_{de0}, h_0, n_s, \epsilon_{re}) \equiv (0.0445, 0.216, 0.740, 0.717, 0.980, 0.092), \quad (4.5)$$

with $\mathcal{A}_{\mathcal{R}} = 2.45 \times 10^{-9}$.

The presence of inflationary magnetic fields affects the CMB observables obtained in the framework of a particular best fit to the WMAP 9yr data for a sufficiently large value of ϵ . This aspect is illustrated in Figs. 2 and 3 where the magnetic fields have been introduced both at the level of the initial conditions and at the level of the evolution equations, as discussed in section 3. Both in Figs. 2 and 3 the fiducial set of Λ CDM parameters has been chosen

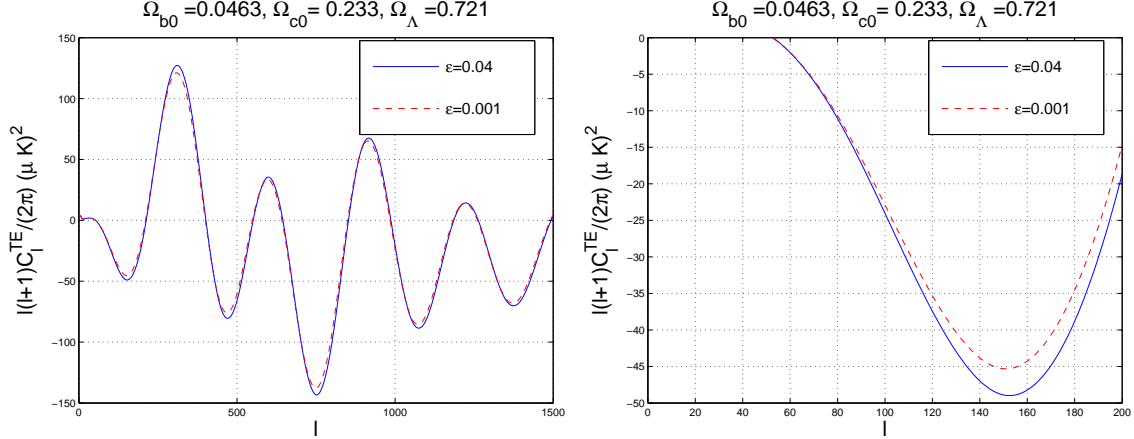


Figure 3: The same cases of Fig. 2 are illustrated in terms of the cross-correlation between temperature and E-mode polarization. At the right the detail of the first anticorrelation peak is illustrated.

as in Eq. (4.3). In the framework of the Λ CDM scenario with standard thermal history the only extra parameter is represented by the slow-roll parameter ϵ : the other parameters controlling the amplitude of the magnetic power spectrum of Eq. (2.7) are determined by the other parameters of the concordance scenario.

In Fig. 2 for sake of simplicity two extreme examples are illustrated, i.e. the case $\epsilon = 0.04$ (full line) and $\epsilon = 0.001$ (dashed line). In the two upper plots of Fig. 2 the TT and EE power spectra are reported, while in the two lower plots of Fig. 2 the angular power spectra appearing in the upper plots have been divided by the best fit to the vanilla Λ CDM model (i.e. in the absence of inflationary magnetic fields). Using the notations of Eq. (4.1) in the two lower plots of Fig. 2 we illustrated, respectively, $\mathcal{G}_\ell^{(TT)}(\epsilon)/\mathcal{G}_\ell^{(TT)}(\epsilon=0)$ and $\mathcal{G}_\ell^{(EE)}(\epsilon)/\mathcal{G}_\ell^{(EE)}(\epsilon=0)$. The shorthand notation $\epsilon=0$ simply means that the corresponding power spectrum is taken to be independent of ϵ , as it happens in the vanilla Λ CDM with no tensors. In Fig. 3 the same analysis has been performed in the case of the TE correlations which cannot be simply divided by the corresponding WMAP 9yr best fit since the TE correlations are not positive definite. To illustrate more closely the differences between the different models, in the right plot of Fig. 3 the first anticorrelation peak has been shown in greater detail.

From Figs. 2 and 3 the case $\epsilon = 0.001$ is practically indistinguishable from the WMAP 9yr bestfit while the case $\epsilon = 0.04$ shows quantitative and qualitative differences potentially jeopardizing the agreement of the computed spectra with the observational data. This disagreement arises since the first, second and third peaks of the acoustic oscillations are distorted. This aspect can be scrutinized from the values of the TT correlations in the neighborhood of the first three acoustic peaks. The position of the peaks will be denoted, respectively, by ℓ_1 , ℓ_2 and ℓ_3 . To pin down the position of the peaks in terms of the Λ CDM

parameters we use the following parametrization adapted to WMAP 9yr data [23]:

$$\ell_j = \bar{\ell}_j + \Delta\ell_j, \quad \bar{\ell}_j = \ell_A(j - \phi_j), \quad (4.6)$$

where ϕ_j and $\Delta\ell_j$ are given, for $j = 1, 2, 3$, as follows:

$$\phi_1 = 0.267 \left(\frac{r_{R*}}{0.3} \right)^{0.1}, \quad \phi_2 = 0.241 \left(\frac{r_{R*}}{0.3} \right)^{0.1}, \quad \phi_3 = 0.353 \left(\frac{r_{R*}}{0.3} \right)^{0.1}, \quad (4.7)$$

$$\Delta\ell_1 = 0.13 |n_s - 1| \bar{\ell}_1, \quad \Delta\ell_2 = 0.33 |n_s - 1| \bar{\ell}_2, \quad \Delta\ell_3 = 0.61 |n_s - 1| \bar{\ell}_3. \quad (4.8)$$

Note that ℓ_A is simply the well known acoustic multipole which is expressible through the angular diameter distance to recombination. Its standard expression can be reduced to a more explicit formula

$$\ell_A = \left(\frac{z_*}{10^3} \right)^{1/2} \frac{\sqrt{R_{b*}} d_A(z_*)}{\ln \left[\frac{\sqrt{1+R_{b*}} + \sqrt{(1+r_{R*})R_{b*}}}{1+\sqrt{r_{R*}R_{b*}}} \right]}, \quad (4.9)$$

where r_{R*} and R_{b*} are given by

$$r_{R*} = \frac{\rho_R(z_*)}{\rho_M(z_*)} = 4.15 \times 10^{-2} (h_0^2 \Omega_M)^{-1} \left(\frac{z_*}{10^3} \right), \quad R_b(z) = \frac{3}{4} \frac{\rho_b}{\rho_\gamma} = 30.36 h_0^2 \Omega_{b0} \left(\frac{10^3}{z_*} \right). \quad (4.10)$$

The quantity z_* is the redshift to recombination which can be directly expressed in terms of Λ CDM parameters as

$$z_* = 1048 [1 + (1.24 \times 10^{-3}) (h_0^2 \Omega_{b0})^{-0.738}] [1 + g_1 (h_0^2 \Omega_{M0})^{g_2}], \quad (4.11)$$

$$g_1 = \frac{0.0783 (h_0^2 \Omega_b)^{-0.238}}{[1 + 39.5 (h_0^2 \Omega_{b0})^{0.763}]}, \quad g_2 = \frac{0.560}{1 + 21.1 (h_0^2 \Omega_{b0})^{1.81}}. \quad (4.12)$$

The parameters of Eq. (4.3) imply $z_* = 1090.95$ in excellent agreement with the estimate of Ref. [16, 17, 18] (i.e. $z_* = 1090.41 \pm 0.57$) in the case of the WMAP 9yr data alone in the light of the vanilla Λ CDM scenario. The relative heights of the acoustic peaks computed in the case of the best-fit of Eq. (4.3) are:

$$\bar{H}_1 = \frac{\mathcal{G}_{\ell_1}^{(TT)}}{\mathcal{G}_{\ell=10}^{(TT)}} = 6.942, \quad \bar{H}_2 = \frac{\mathcal{G}_{\ell_2}^{(TT)}}{\mathcal{G}_{\ell_1}^{(TT)}} = 0.447, \quad \bar{H}_3 = \frac{\mathcal{G}_{\ell_3}^{(TT)}}{\mathcal{G}_{\ell_2}^{(TT)}} = 0.981, \quad (4.13)$$

where $\ell_1 = 221$, $\ell_2 = 538$ and $\ell_3 = 815$ are, respectively, the locations of the first three acoustic peaks obtainable from Eqs. (4.6)–(4.9) and coincide, approximately, with the ones directly obtainable from the angular power spectra. In the case of the angular power spectra illustrated with the full line in the left plots of Fig. 2 the same ratios of Eq. (4.13) are $\bar{H}_1 = 7.35$, $\bar{H}_2 = 0.453$ and $\bar{H}_3 = 0.976$. This shows that the largest effect is on the first peak while the other two are comparatively less affected.

The results obtained in the case of the parameters of Eq. (4.3) are quantitatively and qualitatively close to the results obtainable in the cases of Eqs. (4.4) or (4.5). In Fig. 4,

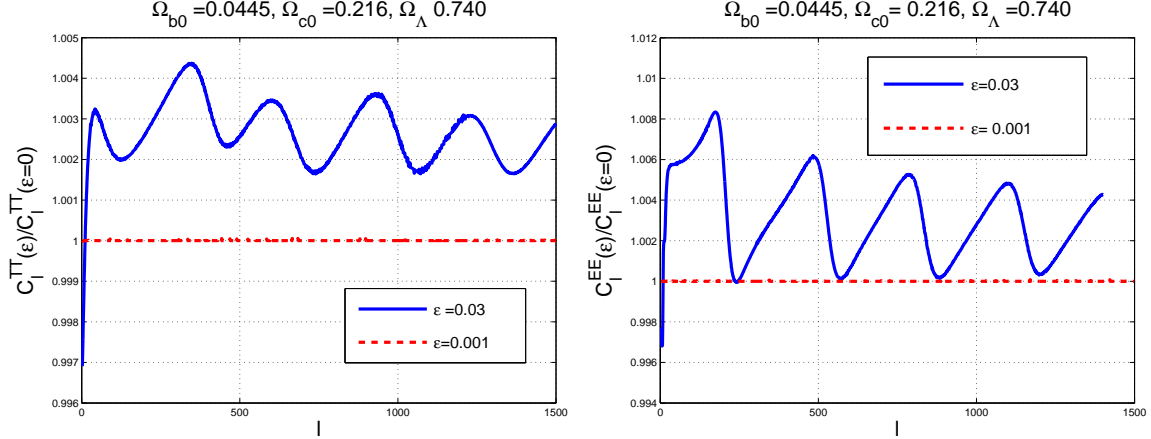


Figure 4: The temperature and polarization autocorrelations divided by the corresponding best fits are illustrated for the fiducial set of parameters reported in Eq. (4.5).

for instance, the parameters of Eq. (4.5) have been assumed while one of the values of ϵ is different. From a closer comparison of Figs. 2 and 4, it can be argued that for $\epsilon < 0.03$ the difference between the magnetized angular power and the corresponding Λ CDM best fit is smaller than 10^{-3} .

In the Λ CDM paradigm without tensors there are no sources of B-mode polarization but a stochastic magnetic field can rotate the polarization plane of the CMB at a rate depending on the difference between the refractive indices associated, respectively, with the positive and with the negative helicities. Faraday rotation is one of the situations where the inadequacy of the one-fluid approximation (for the baryon-lepton fluid) is manifest. The positive and negative helicities composing the (linear) CMB polarization experience, in a background magnetic field, two different phase velocities, two different dielectric constants and, ultimately, two different refractive indices. The mismatch between the refractive index of the positive and negative helicities induces, effectively, a rotation of the CMB polarization and, hence, a B-mode. The inclusion of the Faraday effect in the treatment implies, physically, that the proton-electron fluid (sometimes dubbed as baryon fluid) should be treated as effectively composed by two different species, i.e. the electrons and the ions.

The Faraday effect for the CMB polarization can be treated either with uniform magnetic fields or with stochastic magnetic fields and different analyses have been performed starting with the ones of Ref. [48] (see also [49] for an incomplete list of references). Since the inflationary magnetic fields does not break spatial isotropy, the angular power spectrum of Faraday rotation can be written as:

$$\langle \mathcal{I}(\hat{n}_1) \mathcal{I}(\hat{n}_2) \rangle = \frac{1}{4\pi} \sum_{\ell} (2\ell + 1) C_{\ell}^{(F)} P_{\ell}(\hat{n}_1 \cdot \hat{n}_2), \quad \mathcal{I}(\hat{n}) = \frac{3}{16\pi^2 e} \frac{\hat{n} \cdot \vec{B}}{\nu^2}. \quad (4.14)$$

where $\mathcal{I}(\hat{n})$ is a normalized form of the Faraday rotation rate, ν denotes the comoving frequency and $P_{\ell}(z)$ are the standard Legendre polynomials. In terms of the power spectrum

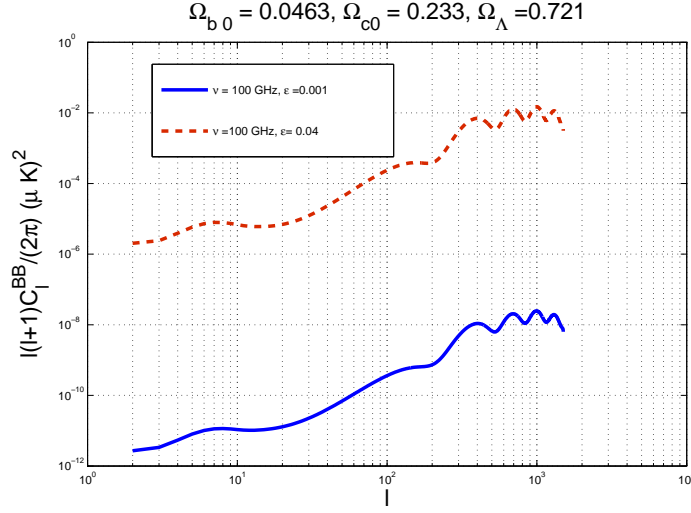


Figure 5: The B-mode polarization power spectrum induced by the Faraday rotation of the E-mode polarization.

of the Faraday rate the autocorrelation of the B-mode polarization can be computed as

$$\mathcal{C}_\ell^{\text{BB}} = \sum_{\ell_1, \ell_2} \mathcal{Z}(\ell, \ell_1, \ell_2) C_{\ell_2}^{\text{EE}} C_{\ell_1}^{(\text{F})} \quad (4.15)$$

where $\mathcal{Z}(\ell, \ell_1, \ell_2)$ is a complicated function of the multipole moments containing also a Clebsch-Gordon coefficient¹⁸ while $C_{\ell_2}^{\text{EE}}$ is the E-mode power spectrum already discussed above.

In Fig. 5 the B-mode autocorrelation is computed in the case of the fiducial set of parameters of Eq. (4.3) and for two illustrative values of ϵ . The Faraday rotation rate depends also on the frequency of observation which has been taken to be 100 GHz. We remind that WMAP experiment observes the microwave sky in five frequency channels (i.e. 23, 33, 41, 61 and 94 in units of GHz). The bandwidth increases from small to high frequencies signaling that probably the best sensitivity to polarization comes the high frequency channels. The WMAP 9yr data do not report any direct detection of the B-mode polarization.

The Planck experiment [50] is observing the microwave sky in nine frequency channels: three frequency channels (i.e. $\nu = 30, 44, 70$ GHz) belong to the low frequency instrument (LFI); six channels (i.e. $\nu = 100, 143, 217, 353, 545, 857$ GHz) belong to the high frequency instrument (HFI). The BB power spectra for all the relevant frequency channels. There are reasons to expect that the sensitivity to polarization will be larger at high frequency [50]. At the same time the expected signal will be larger at small frequencies. We will illustrate the present results for a putative frequency of 100 GHz.

¹⁸For an explicit expression of $\mathcal{Z}(\ell, \ell_1, \ell_2)$ see, for instance, the discussion contained in Appendix C of the last paper quoted in Ref. [49].

The B-mode polarization induced by the tensor modes of the geometry is independent on the frequency channel and for $r_T \sim 0.1$ the induced B-mode polarization ranges between $10^{-3} (\mu\text{K})^2$ and $10^{-2} (\mu\text{K})^2$ which is larger than what we have in Fig. 5 even assuming the maximum value of ϵ . We must however bear in mind that the Faraday rate goes as ν^{-2} and, therefore, C_ℓ^{BB} goes as ν^{-4} . This means that by moving from 100 GHz down to 30 GHz the signal roughly increases by a factor $(10/3)^4 \simeq 123$.

5 Concluding remarks

Often, in the literature, sharp and challenging statements on the interplay of inflationary magnetic fields and CMB anisotropies are not corroborated by detailed analyses. We tried to explore here the opposite perspective by following a more pedantic approach involving the initial conditions of the Einstein-Boltzmann hierarchy in the presence of inflationary seeds. According to some, the really important problem is to tailor specific magnetogenesis mechanisms with very little attention to potentially interesting observational consequences. Some others prefer to assume the existence of large-scale magnetic fields and to scrutinize their phenomenological signatures without bothering to ask why those fields exist. As it has been shown in this paper, the two aforementioned perspectives must be seriously considered as complementary even if they are sometimes viewed as mutually exclusive.

The necessity of bridging the gap between top-down and bottom-up approaches is, fortunately or unfortunately, inherent in all the analyses addressing the interplay of gravitational and gauge interactions in the early Universe. To be fair the same kind of problems emerge in the concordance lore. In this context concordance simply means a minimalistic agreement on the standard completion of the Λ CDM paradigm where the reheating is assumed to be almost sudden, inflation is driven by a single field and the post-inflationary history does not include long phases very different from radiation. Model independent analyses of the large-scale data are desirable but virtually impossible. In this spirit the initial conditions of the Einstein-Boltzmann hierarchy have been derived under the hypothesis that large-scale magnetic fields of inflationary origin were present prior to equality and for typical wavelengths larger than the Hubble radius at the corresponding epoch. Following earlier attempts, the guiding goal of the present investigation is to bring the treatment of magnetized CMB anisotropies to the same standards which are typical of the cases where large-scale magnetic fields are absent.

The main assumption has been that the Λ CDM scenario with standard thermal history and inflationary completion is a sound approximation to the early dynamics of our Hubble patch. Here the amplitude of the magnetic fields is not given extrinsically as a further parameter but it depends on the standard Λ CDM parameters. The parameters of the magnetic power spectrum and hence of the CMB observables only depend on the slow-roll parameter. As an application we presented the explicit computations of the temperature autocorrelations, of the polarization autocorrelations and of the cross-correlation power spectra of temperature and polarization. B-mode autocorrelations are potentially generated by Fara-

day rotation of the CMB whose linear polarization is affected, in turn, by the presence of the magnetic fields.

Let us conclude with a conjecture. The Λ CDM scenario with tensor completion leads to an upper limit on the tensor to scalar ratio r_T . Such a limit, by appropriately combining various data sets ranges from $r_T < 0.3$ down to $r_T < 0.1$. The limit on r_T can be easily translated in a limit on the slow-roll parameter ϵ and then we discover for instance that if $r_T < 0.12$ the modifications induced by the inflationary seed on the temperature and polarization power spectra are indistinguishable from the differences associated with the use of different data bases. Conversely, if we believe that relic magnetic fields are there (and tensors are absent), then the present results suggest that $\epsilon = 0.03$ would already induce observable differences in the CMB spectra and this will imply an independent bound on ϵ possibly achievable with more accurate analyses. In the near future less conventional models of inflationary magnetogenesis can be analyzed by using the same approach developed here.

A Correlation functions

The comoving electric and magnetic fields are defined as

$$\vec{E} = a^2 \sqrt{\lambda} \vec{e}, \quad \vec{B} = a^2 \sqrt{\lambda} \vec{b}. \quad (\text{A.1})$$

The fields \vec{e} and \vec{b} are introduced from the corresponding field strengths, i.e. $Y_{i0} = -a^2 e_i$ and $Y_{ij} = -a^2 \epsilon_{ijk} b^k$. The gauge action is canonical in terms of \vec{E} and \vec{B} and not in terms of \vec{e} and \vec{b} . The evolution equations of the canonical modes derived from the action and their explicit form is:

$$\frac{1}{\sqrt{\lambda}} \vec{\nabla} \cdot (\sqrt{\lambda} \vec{E}) = 0, \quad \sqrt{\lambda} \vec{\nabla} \cdot \left(\frac{\vec{B}}{\sqrt{\lambda}} \right) = 0, \quad (\text{A.2})$$

$$\frac{1}{\sqrt{\lambda}} \vec{\nabla} \times (\sqrt{\lambda} \vec{B}) = \vec{J} + \frac{1}{\sqrt{\lambda}} \frac{\partial}{\partial \tau} (\sqrt{\lambda} \vec{E}), \quad (\text{A.3})$$

$$\sqrt{\lambda} \vec{\nabla} \times \left(\frac{\vec{E}}{\sqrt{\lambda}} \right) = -\sqrt{\lambda} \frac{\partial}{\partial \tau} \left(\frac{\vec{B}}{\sqrt{\lambda}} \right), \quad (\text{A.4})$$

where the possible presence of the Ohmic current has been included for completeness even if conducting initial conditions will not be considered explicitly. The system of Eqs. (A.2)–(A.4), in the absence of electromagnetic sources, is invariant under the generalized duality transformation $\vec{E} \rightarrow -\vec{B}$, $\vec{B} \rightarrow \vec{E}$ and $\sqrt{\lambda} \rightarrow 1/\sqrt{\lambda}$ [37, 38]. The conventions for the Fourier transform are:

$$B_i(\vec{x}, \tau) = \frac{1}{(2\pi)^{3/2}} \int d^3k B_i(\vec{k}, \tau) e^{-i\vec{k} \cdot \vec{x}}, \quad E_i(\vec{x}, \tau) = \frac{1}{(2\pi)^{3/2}} \int d^3k E_i(\vec{k}, \tau) e^{-i\vec{k} \cdot \vec{x}}. \quad (\text{A.5})$$

Consequently the fluctuations of the magnetic and electric energy densities is given by:

$$\begin{aligned} \delta\rho_B(\vec{q}, \tau) &= \frac{1}{(2\pi)^{3/2} 8\pi a^4} \int d^3k \left[B_i(\vec{k}, \tau) B_i(\vec{q} - \vec{k}, \tau) - \frac{4\pi^2}{k^3} P_B(k, \tau) \delta^{(3)}(\vec{q}) \right], \\ \delta\rho_E(\vec{q}, \tau) &= \frac{1}{(2\pi)^{3/2} 8\pi a^4} \int d^3k \left[E_i(\vec{k}, \tau) E_i(\vec{q} - \vec{k}, \tau) - \frac{4\pi^2}{k^3} P_E(k, \tau) \delta^{(3)}(\vec{q}) \right]. \end{aligned} \quad (\text{A.6})$$

The electric and magnetic anisotropic stresses are defined as

$$\begin{aligned} \Pi_{ij}^{(B)}(\vec{q}, \tau) &= \frac{1}{4\pi a^4} \int \frac{d^3k}{(2\pi)^{3/2}} \left[B_i(\vec{k}, \tau) B_j(\vec{q} - \vec{k}, \tau) - \frac{\delta_{ij}}{3} B_m(\vec{k}, \tau) B_m(\vec{q} - \vec{k}, \tau) \right], \\ \Pi_{ij}^{(E)}(\vec{q}, \tau) &= \frac{1}{4\pi a^4} \int \frac{d^3k}{(2\pi)^{3/2}} \left[E_i(\vec{k}, \tau) E_j(\vec{q} - \vec{k}, \tau) - \frac{\delta_{ij}}{3} E_m(\vec{k}, \tau) E_m(\vec{q} - \vec{k}, \tau) \right]. \end{aligned} \quad (\text{A.7})$$

The stochastic averages of the fluctuations variables defined in Eqs. (A.6)–(A.7) are all vanishing, i.e. using Eqs. (2.5)–(2.6), $\langle \delta\rho_B(\vec{x}, \tau) \rangle = 0$ and $\langle \delta\rho_E(\vec{x}, \tau) \rangle = 0$ and similarly for

the anisotropic stresses. The second order correlations of the magnetic energy density and of the anisotropic stress are

$$\langle \delta \rho_B(\vec{q}, \tau) \delta \rho_B(\vec{p}, \tau) \rangle = \frac{2\pi^2}{q^3} \mathcal{Q}_B(q, \tau) \delta^{(3)}(\vec{q} + \vec{p}), \quad (\text{A.8})$$

$$\langle \Pi_B(\vec{q}, \tau) \Pi_B(\vec{p}, \tau) \rangle = \frac{2\pi^2}{q^3} \mathcal{Q}_{B\Pi}(q, \tau) \delta^{(3)}(\vec{q} + \vec{p}), \quad (\text{A.9})$$

where

$$\mathcal{Q}_B(q, \tau) = \frac{q^3}{128 \pi^3 a^8} \int d^3 k \frac{P_B(k, \tau)}{k^3} \frac{P_B(|\vec{q} - \vec{k}|, \tau)}{|\vec{q} - \vec{k}|^3} \Lambda_\rho(k, q), \quad (\text{A.10})$$

$$\mathcal{Q}_{B\Pi}(q, \tau) = \frac{q^3}{288 \pi^3 a^8(\tau)} \int d^3 k \frac{P_B(k, \tau)}{k^3} \frac{P_B(|\vec{q} - \vec{k}|, \tau)}{|\vec{q} - \vec{k}|^3} \Lambda_\Pi(k, q). \quad (\text{A.11})$$

The functions $\Lambda_\rho(k, q)$ and $\Lambda_\Pi(k, q)$ are defined as

$$\Lambda_\rho(k, q) = 1 + \frac{[\vec{k} \cdot (\vec{q} - \vec{k})]^2}{k^2 |\vec{q} - \vec{k}|^2}, \quad (\text{A.12})$$

$$\begin{aligned} \Lambda_\Pi(k, q) = & 1 + \frac{[\vec{k} \cdot (\vec{q} - \vec{k})]^2}{k^2 |\vec{q} - \vec{k}|^2} + \frac{6}{q^2} \left[\vec{k} \cdot (\vec{q} - \vec{k}) - \frac{[\vec{k} \cdot (\vec{q} - \vec{k})]^3}{k^2 |\vec{q} - \vec{k}|^2} \right] \\ & + \frac{9}{q^4} \left[k^2 |\vec{q} - \vec{k}|^2 - 2[\vec{k} \cdot (\vec{q} - \vec{k})]^2 + \frac{[\vec{k} \cdot (\vec{q} - \vec{k})]^4}{k^2 |\vec{q} - \vec{k}|^2} \right]. \end{aligned} \quad (\text{A.13})$$

The functions $\Lambda_\rho(k, q)$ and $\Lambda_\Pi(k, q)$ coincide for magnetic and electric degrees of freedom since both \vec{E} and \vec{B} are solenoidal fields: \vec{B} is solenoidal because of the absence of magnetic monopoles while \vec{E} is solenoidal because the protoinflationary plasma is globally neutral and any electric charge asymmetry is absent. The explicit expressions of the power spectra of Eqs. (A.10) and (A.11) is obtained by using the power spectra of Eqs. (2.2)–(2.3).

For typical wavelengths larger than the Hubble radius the second-order spectra including the slow roll corrections are given by:

$$\mathcal{Q}_B(q, \tau) = \mathcal{O}_B(q, \epsilon, f) \left(\frac{a}{a_{ex}} \right)^{g_B(\epsilon, f)}, \quad \mathcal{Q}_{B\Pi}(q, \tau) = \mathcal{O}_{B\Pi}(q, \epsilon, f) \left(\frac{a}{a_{ex}} \right)^{g_B(\epsilon, f)}, \quad (\text{A.14})$$

where $g_B(\epsilon, f) = 4f - 8 + 4\epsilon f$. The k -dependent amplitudes appearing in Eqs. (A.14) are:

$$\begin{aligned} \mathcal{O}_B(q, \epsilon, f) &= H^8 \mathcal{C}_B(f, \epsilon) \mathcal{L}_B(f, \epsilon, q) \left(\frac{q}{q_p} \right)^{m_B(\epsilon, f) - 1}, \\ \mathcal{O}_{B\Pi}(q, \epsilon, f) &= H^8 \mathcal{C}_{B\Pi}(f, \epsilon) \mathcal{L}_{B\Pi}(f, \epsilon, q) \left(\frac{q}{q_p} \right)^{m_{B\Pi}(\epsilon, f) - 1}, \end{aligned} \quad (\text{A.15})$$

where $m_B(\epsilon, f) = m_{B\Pi}(\epsilon, f) = 9 - 4f(1 + \epsilon)$. The functions $\mathcal{C}_B(f, \epsilon)$ and $\mathcal{C}_{B\Pi}(f, \epsilon)$ are given, respectively, by:

$$\mathcal{C}_B(f, \epsilon) = \frac{2^{4f(1+\epsilon)}}{1024 \pi^7} \Gamma^4[f(1 + \epsilon) + 1/2], \quad \mathcal{C}_{B\Pi}(f, \epsilon) = \frac{4}{9} \mathcal{C}_B(f, \epsilon). \quad (\text{A.16})$$

The functions $\mathcal{L}_B(f, \epsilon, q)$ and $\mathcal{L}_{B\Pi}(f, \epsilon, q)$ are:

$$\begin{aligned}\mathcal{L}_B(f, \epsilon, q) &= \frac{8[f(1+\epsilon)+1]}{3[4f(1+\epsilon)-5][4-2f(1+\epsilon)]} - \frac{8}{3[4-2f(1+\epsilon)]} \left(\frac{q}{q_0}\right)^{2f(1+\epsilon)-4} \\ &+ \frac{4}{5-4f(1+\epsilon)} \left(\frac{q}{q_{\max}}\right)^{4f(1+\epsilon)-5},\end{aligned}\quad (\text{A.17})$$

$$\begin{aligned}\mathcal{L}_{B\Pi}(f, \epsilon, q) &= \frac{2[17-2f(1+\epsilon)]}{15[4f(1+\epsilon)-5][4-2f(1+\epsilon)]} - \frac{2}{3[4-2f(1+\epsilon)]} \left(\frac{q}{q_0}\right)^{2f(1+\epsilon)-4} \\ &+ \frac{7}{5-4f(1+\epsilon)} \left(\frac{q}{q_{\max}}\right)^{4f(1+\epsilon)-5},\end{aligned}\quad (\text{A.18})$$

The comoving scale $q_p = 0.002 \text{ Mpc}^{-1}$ is the usual pivot scale at which the power spectra of the scalar curvature are assigned. The value of q_0 has been chosen $0.001 q_p$ while q_{\max} is related to the maximal amplified frequency of the magnetic field spectrum.

B Evolution equations in the α parametrization.

In the α -parametrization the Hamiltonian and the momentum constraints read, respectively,

$$\frac{\partial h}{\partial \alpha} = \frac{\kappa^2 \alpha}{2(\alpha+1)} \xi - \frac{3}{\alpha} \left[\Omega_R \left(R_\nu \delta_\nu + R_\gamma \delta_\gamma \right) + \Omega_M \left(\frac{\Omega_{c0}}{\Omega_{M0}} \delta_c + \frac{\Omega_{b0}}{\Omega_{M0}} \delta_b \right) \right], \quad (\text{B.1})$$

$$\kappa^2 \alpha^2 \frac{\partial \xi}{\partial \alpha} = -\frac{4}{\sqrt{\alpha+1}} \left\{ R_\nu \theta_\nu + R_\gamma [1 + R_b(\alpha)] \theta_{\gamma b} + \frac{3}{4} \frac{\Omega_{c0}}{\Omega_{M0}} \alpha \theta_c \right\}. \quad (\text{B.2})$$

where $R_b(\alpha)$ denote the baryon-to-photon ratio $R_b(\alpha) = 3(\Omega_{b0}/\Omega_{M0}) \alpha / (4R_\gamma) \simeq 0.215 \alpha$. The remaining two equations stemming from the perturbed Einstein equations can be written as:

$$\frac{\partial^2 h}{\partial \alpha^2} + \frac{5\alpha+4}{2\alpha(\alpha+1)} \frac{\partial h}{\partial \alpha} - \frac{\kappa^2 \xi}{2(\alpha+1)} = \frac{3}{\alpha^2(\alpha+1)} \left[R_\gamma \delta_\gamma + R_\nu \delta_\nu + R_\gamma \Omega_B \right], \quad (\text{B.3})$$

$$\frac{\partial^2 \mathcal{Q}}{\partial \alpha^2} + \frac{5\alpha+4}{2\alpha(\alpha+1)} \frac{\partial \mathcal{Q}}{\partial \alpha} = \frac{\kappa^2 \xi}{2(\alpha+1)} + \frac{12}{\alpha^2(\alpha+1)} (R_\nu \sigma_\nu + R_\gamma \sigma_B). \quad (\text{B.4})$$

where $\mathcal{Q} = (h + 6\xi)$; the evolution equations of the neutrinos obey,

$$\frac{\partial \delta_\nu}{\partial \alpha} = -\frac{2\theta_\nu}{3\sqrt{\alpha+1}} + \frac{2}{3} \frac{\partial h}{\partial \alpha}, \quad \frac{\partial \theta_\nu}{\partial \alpha} = \frac{\kappa^2}{8\sqrt{\alpha+1}} \delta_\nu - \frac{\kappa^2}{2\sqrt{\alpha+1}} \sigma_\nu, \quad (\text{B.5})$$

$$\frac{\partial \sigma_\nu}{\partial \alpha} = \frac{2\theta_\nu}{15\sqrt{\alpha+1}} - \frac{2}{15} \frac{\partial \mathcal{Q}}{\partial \alpha} - \frac{3}{20} \frac{\kappa \mathcal{F}_{\nu 3}}{\sqrt{\alpha+1}}, \quad (\text{B.6})$$

$$\frac{\partial \mathcal{F}_{\nu \ell}}{\partial \alpha} = \frac{\kappa}{2(2\ell+1)\sqrt{\alpha+1}} [\ell \mathcal{F}_{\nu(\ell-1)} - (\ell+1) \mathcal{F}_{\nu(\ell+1)}], \quad \ell \geq 3 \quad (\text{B.7})$$

The evolution equations of the dark-matter sector obey instead

$$\frac{\partial \delta_c}{\partial \alpha} = -\frac{\theta_c}{2\sqrt{\alpha+1}} + \frac{1}{2} \frac{\partial h}{\partial \alpha}, \quad \frac{\partial \theta_c}{\partial \alpha} + \frac{\theta_c}{\alpha} = 0 \quad (\text{B.8})$$

In the tight-coupling approximation the equations of the baryon-photon system are:

$$\frac{\partial \theta_{\gamma\text{b}}}{\partial \alpha} + \frac{R_{\text{b}} \theta_{\gamma\text{b}}}{\alpha(R_{\text{b}} + 1)} = \frac{\kappa^2 \delta_{\gamma}}{8\sqrt{\alpha+1}(R_{\text{b}} + 1)} + \frac{\kappa^2 (\Omega_{\text{B}} - 4\sigma_{\text{B}})}{8\sqrt{\alpha+1}(R_{\text{b}} + 1)}, \quad (\text{B.9})$$

$$\frac{\partial \delta_{\gamma}}{\partial \alpha} = -\frac{2}{3} \frac{\theta_{\gamma\text{b}}}{\sqrt{\alpha+1}} + \frac{2}{3} \frac{\partial h}{\partial \alpha}, \quad \frac{\partial \delta_{\text{b}}}{\partial \alpha} = -\frac{\theta_{\gamma\text{b}}}{2\sqrt{\alpha+1}} + \frac{1}{2} \frac{\partial h}{\partial \alpha}. \quad (\text{B.10})$$

References

- [1] E. Fermi, Phys. Rev. **75**, 1169 (1949).
- [2] H. Alfvén, Phys. Rev. **75**, 1732 (1949); R. D. Richtmyer and E. Teller, Phys. Rev. **75**, 1729 (1949).
- [3] W. A. Hiltner, Science **109**, 165 (1949); J. S. Hall: Science **109**, 166 (1949).
- [4] L. J. Davis and J. L. Greenstein, Astrophys. J. **114**, 206 (1951).
- [5] G. Cocconi, Phys. Rev. Phys. Rev. **83**, 1193 (1951).
- [6] R. Beck, Space Sci. Rev. **99**, 243 (2001).
- [7] C. L. Carilli and G. B. Taylor, Ann. Rev. Astron. Astrophys. **40**, 319 (2002); T. E. Clarke, P. P. Kronberg and H. Boehringer, Astrophys. J. **547**, L111 (2001).
- [8] Y. Xu, P. P. Kronberg, S. Habib and Q. W. Dufton, Astrophys. J. **637**, 19 (2006).
- [9] P. Abreu *et al.* [Pierre Auger Collaboration], Astrophys. J. Lett., 762, L **13** (2012).
- [10] J. Abraham *et al.* [Pierre Auger Collaboration], Science **318**, 938 (2007).
- [11] M. Aglietta *et al.* [Pierre Auger Collaboration], Astropart. Phys. **27**, 244 (2007).
- [12] E. Harrison, Phys. Rev. Lett. **18**, 1011 (1967); Phys. Rev. **167**, 1170 (1968).
- [13] Ya. Zeldovich, Sov. Phys. JETP **21**, 656 (1965); Ya. Zeldovich and I. Novikov, *The structure evolution of the Universe* (Chicago University Press, Chicago, 1971), Vol. 2.
- [14] E. Parker, *Cosmical Magnetic Fields* (Oxford University Press, Oxford, 1979); K. Enqvist, Int. J. Mod. Phys. D **7**, 331 (1998); M. Giovannini, Int. J. Mod. Phys. D **13**, 391 (2004); J. D. Barrow, R. Maartens and C. G. Tsagas, Phys. Rept. **449**, 131 (2007).
- [15] M. Giovannini, Phys. Rev. D **62**, 123505 (2000).
- [16] G. Hinshaw, *et al.*, arXiv:1212.5226 [astro-ph.CO]; C. L. Bennett, *et al.*, arXiv:1212.5225 [astro-ph.CO].
- [17] C. L. Bennett *et al.*, Astrophys. J. Suppl. **192**, 17 (2011); N. Jarosik *et al.*, Astrophys. J. Suppl. **192**, 14 (2011); J. L. Weiland *et al.*, Astrophys. J. Suppl. **192**, 19 (2011); D. Larson *et al.*, Astrophys. J. Suppl. **192**, 16 (2011); B. Gold *et al.*, Astrophys. J. Suppl. **192**, 15 (2011); E. Komatsu *et al.*, Astrophys. J. Suppl. **192**, 18 (2011).
- [18] D. N. Spergel *et al.*, Astrophys. J. Suppl. **170**, 377 (2007); D. N. Spergel *et al.* Astrophys. J. Suppl. **148**, 175 (2003) [astro-ph/0302209].

- [19] M. Giovannini, *Class. Quant. Grav.* **23**, R1 (2006).
- [20] A. G. Riess *et al.* [Supernova Search Team Collaboration], *Astrophys. J.* **607**, 665 (2004); B. J. Barris *et al.*, *Astrophys. J.* **602**, 571 (2004); P. Astier *et al.* [The SNLS Collaboration], *Astron. Astrophys.* **447**, 31 (2006).
- [21] M. Hicken *et al.*, *Astrophys. J.* **700**, 1097 (2009); A. Conley *et al.*, *Astrophys. J. Suppl.* **192**, 1 (2011); M. Sullivan *et al.*, *Astrophys. J.* **737**, 102 (2011).
- [22] D. J. Eisenstein *et al.* [SDSS Collaboration], *Astrophys. J.* **633**, 560 (2005); W. J. Percival, *et al.* *Mon. Not. Roy. Astron. Soc.* **381**, 1053 (2007).
- [23] M. Giovannini, *Class. Quant. Grav.* **27**, 105011 (2010); *Phys. Rev. D* **79**, 103007 (2009); *Phys. Rev. D* **79**, 121302 (2009).
- [24] V. N. Lukash, *Sov. Phys. JETP* **52**, 807 (1980) [*Zh. Eksp. Teor. Fiz.* **79**, 1601 (1980)].
- [25] E. M. Lifshitz and I. M. Khalatnikov, *Adv. Phys.* **12**, 185 (1963); E. M. Lifshitz *Zh. Eksp. Teor. Fiz.* **16**, 587 (1946).
- [26] V. Strokov, *Astron. Rep.* **51**, 431-434 (2007).
- [27] V. N. Lukash and I. D. Novikov, *Lectures on the very early universe in Observational and Physocal Cosmology*, II Canary Islands Winter School of Astrophysics, eds. F. Sanchez, M. Collados and R. Rebolo (Cambridge University Press, Cambridge UK, 1992), p. 3.
- [28] J. Bardeen, *Phys. Rev.* **D22**, 1882 (1980).
- [29] H. Kodama, M. Sasaki, *Prog. Theor. Phys. Suppl.* **78**, 1-166 (1984); M. Sasaki, *Prog. Theor. Phys.* **76**, 1036 (1986).
- [30] G. V. Chibisov, V. F. Mukhanov, *Mon. Not. Roy. Astron. Soc.* **200**, 535 (1982); V. F. Mukhanov, *Sov. Phys. JETP* **67**, 1297 (1988) [*Zh. Eksp. Teor. Fiz.* **94**, 1 (1988)].
- [31] R. H. Brandenberger, R. Kahn and W. H. Press, *Phys. Rev. D* **28**, 1809 (1983); R. H. Brandenberger and R. Kahn, *Phys. Rev. D* **29**, 2172 (1984).
- [32] J. Bardeen, P. Steinhardt, and M. Turner, *Phys. Rev.* **D28**, 679 (1983); J. A. Frieman and M. S. Turner, *Phys. Rev. D* **30**, 265 (1984).
- [33] M. Giovannini, *Phys. Rev. D* **64**, 061301 (2001); *Phys. Lett. B* **659**, 661 (2008); *JCAP* **1004**, 003 (2010).
- [34] K. Bamba and M. Sasaki, *JCAP* **02**, 030 (2007); K. Bamba, *Phys. Rev. D* **75** 083516 (2007).

- [35] M. Giovannini, Phys. Rev. D **85**, 101301 (2012); Phys. Rev. D **86**, 103009 (2012).
- [36] M. Giovannini, CERN-TH-PH/2012-367, arXiv:1302.2243 [hep-th].
- [37] S. Deser and C. Teitelboim, Phys. Rev. D **13**, 1592 (1976).
- [38] S. Deser, J. Phys. A **15**, 1053 (1982).
- [39] P. J. E. Peebles and J. T. Yu, Astrophys. J. **162** 815 (1970).
- [40] E. Bertschinger, *COSMICS* arXiv:astro-ph/9506070; C. P. Ma and E. Bertschinger, Astrophys. J. **455**, 7 (1995)
- [41] U. Seljak and M. Zaldarriaga, Astrophys. J. **469**, 437 (1996); M. Zaldarriaga, D. N. Spergel and U. Seljak, Astrophys. J. **488**, 1 (1997).
- [42] W. Press and E. Vishniac, Astrophys. J. **239**, 1 (1980); Astrophys. J. **236**, 323 (1980).
- [43] W. J. Percival *et al.* [SDSS Collaboration], Mon. Not. Roy. Astron. Soc. **401**, 2148 (2010).
- [44] J. Dunkley, R. Hlozek, J. Sievers, V. Acquaviva, P. A. R. Ade, P. Aguirre, M. Amiri and J. W. Appel *et al.*, Astrophys. J. **739**, 52 (2011).
- [45] R. Keisler, C. L. Reichardt, K. A. Aird, B. A. Benson, L. E. Bleem, J. E. Carlstrom, C. L. Chang and H. M. Cho *et al.*, Astrophys. J. **743**, 28 (2011).
- [46] J. Guy, M. Sullivan, A. Conley, N. Regnault, P. Astier, C. Balland, S. Basa and R. G. Carlberg *et al.* Astron. Astrophys. **523**, A7 (2010).
- [47] H. Heiselberg, Phys. Rev. D **49**, 4739 (1994); J. Ahonen and K. Enqvist, Phys. Lett. B **382**, 40 (1996); J. Ahonen, Phys. Rev. D **59**, 023004 (1999).
- [48] A. Kosowsky and A. Loeb, Astrophys. J. **469**, 1 (1996); D. D. Harari, J. D. Hayward and M. Zaldarriaga, Phys. Rev. D **55**, 1841 (1997); M. Giovannini, Phys. Rev. D **56**, 3198 (1997).
- [49] C. Scoccola, D. Harari and S. Mollerach, Phys. Rev. D **70**, 063003 (2004); L. Campanelli, A. D. Dolgov, M. Giannotti and F. L. Villante, Astrophys. J. **616**, 1 (2004); A. Kosowsky, T. Kahniashvili, G. Lavrelashvili and B. Ratra, Phys. Rev. D **71**, 043006 (2005). M. Giovannini, Phys. Rev. D **71**, 021301 (2005); M. Giovannini and K. E. Kunze, Phys. Rev. D **79**, 063007 (2009); Phys. Rev. D **78**, 023010 (2008).
- [50] See, for instance, <http://www.rssd.esa.int/index.php?project=PLANCK> for the updated scientific case of the Planck experiment and for the last version of the scientific program.